THESIS FOR THE DEGREE OF LICENTIATE OF ENGINEERING

Fate of Trace Elements in Thermochemical Conversion of Waste Fuels Using Oxygen Carriers

IVANA STANIČIĆ

Department of Space, Earth and Environment

CHALMERS UNIVERSITY OF TECHNOLOGY

Gothenburg, Sweden 2021

Fate of Trace Elements in Thermochemical Conversion of Waste Fuels Using Oxygen Carriers

IVANA STANIČIĆ

Department of Space, Earth and Environment
Division of Energy Technology
Chalmers University of Technology
SE-412 96 Gothenburg
Sweden
Telephone + 46 (0)31-772 1000

Printed by Chalmers Reproservice
Gothenburg, Sweden 2021

Fate of Trace Elements in Thermochemical Conversion of Waste Fuels Using Oxygen Carriers

IVANA STANIČIĆ

Division of Energy Technology

Department of Space, Earth and Environment

Chalmers University of Technology

Abstract

The metals zinc, copper and lead are amongst the more abundant trace elements in waste fuels. The fate of these elements is important to study because they can affect the thermochemical conversion process and end up in ashes. With respect to the latter, this could have environmental implications when the ashes are used or landfilled but may also open up for the possibility of recycling. Utilizing metal oxides, so called oxygen carriers, as bed material in fluidized bed combustion could affect the fate of these metals. The interaction between heavy metals and oxygen carriers is an unexplored field of research. In this thesis a combined theoretical and experimental approach is used to study the fate of Zn, Cu and Pb in presence of oxygen carriers. Analysis methods such as scanning electron microscopy and x-ray diffraction were utilized to study morphology and main crystalline phases. Due to low concentrations x-ray photoelectron spectroscopy (XPS) was also used to study the trace elements on the surface and cross section of oxygen carrier particles. Thermodynamic calculations and a user defined database were applied to study phase formation for a range of parameters.

Solid samples were obtained from industrial fluidized bed applications using oxygen carriers. The availability of samples from commercial units burning wastes provided a unique opportunity to study the trace element chemistry, as the long residence times of solids will allow for sufficient trace element interaction to be able to characterize appropriately. Analyzing ilmenite particles revealed incorporation of Zn the ash layer and accumulation of Cu inside the particles. During chemical looping gasification of a metal rich fuel and olivine, one major observation related to the surface enrichment of Cu and Zn, also in the form of ferrites. Thus, Fe is shown to play an important role for the interaction between the bed material and Cu and Zn. Pb is mainly concentrated in the fly ashes, during both olivine and ilmenite operation, although some lead chlorides, silicates and/or titanates were identified on the particles. Experimental findings and thermodynamic calculations indicate that the trace element chemistry is not only dependent on the oxygen carrier but also other ash components, for example K, Si and Cl. The proposed methodology in this thesis and the knowledge gained, can be applicable for other technologies using oxygen carriers, for example chemical looping combustion.

Keywords: Oxygen Carriers, Trace Elements, Ash interaction, Thermodynamic Calculations, Oxygen Carrier Aided Combustion, Waste, Ilmenite, Oxygen Carrier Aided Combustion, Chemical Looping Technologies, X-ray Photoelectron Spectroscopy

Acknowledgements

I would like to express my deepest appreciation to Professor Tobias Mattisson for the valuable discussions and constructive feedback during the planning and development of this research. Thank you for believing in me and challenging me. I would also like to extend my gratitude to Professor Rainer Backman who has been involved since the beginning of this project. Thank you for the guidance and in-depth thermodynamic discussions, your contribution has been invaluable. I also want to express my gratitude to Associate Professor Yu Cao and Professor Magnus Rydén. Thank you, Yu, for the valuable feedback and support in the lab and thank you, Magnus, for your inputs to the papers and understanding of the bigger picture.

Formas, Swedish Research Council for Environment, Agricultural Sciences and Spatial Planning, is acknowledged for the financial support of this work (2017-01095). I would also like to thank E.ON/Improbed for providing the opportunity to study materials from their facilities. A special thanks to Fredrik Lind, Patrick Moldenhauer and Jesper Aronsson for the support and help with sampling.

This thesis would not have been completed without the help of my co-authors and colleagues. Thank you, Henrik Leion, Jelena Maric, Isabel Cañete Vela and Pavleta Knutsson for sharing knowledge and working with me. I also want to thank Fredrik Normann and Termogänget. It has been a pleasure to be a part of this teaching group. I am grateful for my colleagues at Energy Technology, department of Chemistry and Chemical Engineering, and Industrial and Materials Science. I look forward to continuing my PhD journey with all of you.

Thank you, Viktor Andersson, for your support as a dear friend and colleague, I'm grateful for sharing this journey with you.

To my parents, sister, and brother whose support and faith brought me here, thank you. Finally, to my inspiration and motivation. Amer, I am grateful for your unfailing support and continuous encouragement.

Ivana Staničić, Göteborg 2021

List of Publications

This thesis is based on the work contained in the following papers, referred to by Roman numerals in the text:

Paper I
Staničić I., Hanning M., Deniz R., Mattisson T., Backman R., Leion H. (2020)
Interaction of oxygen carriers with common biomass ash components.
Fuel Processing Technology. 200:106313.

Paper II
Staničić I., Mattisson T., Backman R., Cao Y., Rydén M. (2021)
Oxygen Carrier Aided Combustion (OCAC) of Two Waste Fuels – Experimental and Theoretical Study of the Interaction between Ilmenite and Zinc, Copper and Lead
*Biomass and Bioenergy.*148:106060

Paper III
Staničić I., Backman R., Cao Y., Rydén M., Aronsson J., Mattisson T.
Fate of Trace Elements in a Time Series of Samples from Oxygen Carrier Aided Combustion (OCAC) of Municipal Solid Waste
Submitted for publication (2021)

Paper IV
Staničić I., Cañete Vela I., Backman R., Maric J., Cao Y., Mattisson T.
Fate of Lead, Copper and Zinc during Chemical Looping Gasification of Automotive Shredder Residue
Submitted for publication (2021)

Contribution report:

Paper I	Principal author, responsible for data evaluation, thermodynamic calculations and writing
Paper II	Principal author, responsible for experimental work, data evaluation, thermodynamic calculations and writing
Paper III	Principal author, responsible for experimental work, data evaluation, thermodynamic calculations and writing
Paper IV	Principal author, responsible for experimental work, data evaluation, thermodynamic calculations and writing

Related peer-reviewed papers not included in this thesis

Staničić I., Andersson V., Hanning M., Mattisson T., Backman R., Leion H. (2019). Combined manganese oxides as oxygen carriers for biomass combustion — Ash interactions. *Chemical Engineering Research and Design*, 149:104-20.

Table of Contents

1. Introduction

The concentrations of greenhouse gases in the atmosphere are increasing as a result of anthropogenic activities. The main reason is the extensive use of fossil fuels where a quarter of the total emission originate from the production of electricity and heat [1]. As a result, the global mean temperature has increased with subsequent climate change. The warming from these anthropogenic emissions will persist from centuries to millennia and cause long term changes in the climate system [2]. In order to reach the climate goals and limit the warming to 1.5℃ from pre-industrial levels it is necessary to actively remove carbon dioxide from the atmosphere [3]. Carbon Capture and Storage (CCS) is essential technology for this purpose. To mitigate the greenhouse gas effect, one needs to consider energy sources beyond fossil fuels. In addition to solar and wind-energy, biomass is one important option. Utilizing biomass for combustion provides a possibility for carbon dioxide neutral or even negative emissions. With respect to the latter, Bio-Energy with Carbon Capture and Storage (BECCS) is necessary in order to achieve negative greenhouse gas emissions, essential for limiting the global warming [4, 5].

The second largest contributor to the greenhouse gas emissions is methane, which has a global warming potential GWP_{100} = 28 [6, 7]. One of the largest anthropogenic sources of methane emissions originate from waste landfills [8]. When municipal solid waste (MSW) is landfilled, the biodegradable portion releases methane and CO_2 into the atmosphere. Globally, MSW has been mainly managed in form of landfilling in open dump sites, followed by recycling and thermal treatment [9]. However, since the beginning of the 21st century, disposal of waste in landfills has been reduced by more than half in the EU as a result of the Waste Framework Directive (2008/98/EC) and Landfill Directive (Council Directive 1999/31/EC) while incineration with energy recovery has increased fourfold [10]. The Waste Framework Directive (2008/98/EC) collects the main concepts related to waste management. The waste hierarchy, presented in Figure 1, defines a priority order for different management options going from the most desired option - prevention, to the least desired option – disposal.

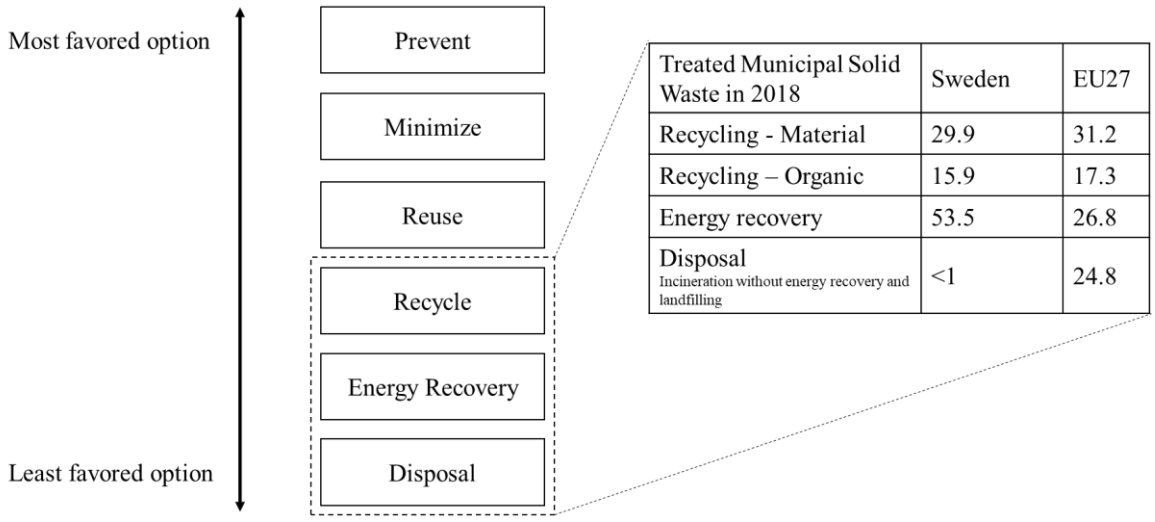

Treated Municipal Solid Waste in 2018	Sweden	EU27
Recycling - Material	29.9	31.2
Recycling – Organic	15.9	17.3
Energy recovery	53.5	26.8
Disposal Incineration without energy recovery and landfilling	<1	24.8

Figure 1. The waste management hierarchy along with the different treatment processes for municipal solid waste. Data for treated waste in Sweden and EU in wt % compiled from Eurostat [10].

When prevention, minimization, reusage and recycling are not feasible options, energy recovery becomes preferred over disposal [11]. EU regulations regarding waste management and landfilling are constantly being updated with new strict targets encouraging Europe's transition towards a circular economy. The landfilling targets (1999/31/EU) aims to phase out landfilling, and it includes a ban of separately collected waste and a target of reducing landfilling of

municipal solid waste to below 10% by 2030. The global waste generation is expected to increase from 2.0 billion tons (2016) to 3.4 billion tons by 2050 [9, 12] which may be attributed to increasing population and economic growth [12]. This will require handling of large volumes of waste. In addition, the global Waste-to-Energy (WtE) technology markets can be expected to increase drastically along with the increasing energy demand. Incineration of waste provides renewable energy benefits while producing minor GHG-emissions compared with landfilling [6]. Furthermore it can decrease the volume of waste flows by 70 wt% and it's beneficial from a hygienic point of view [13].

Sweden has an extensive and efficient waste management systems and landfills are almost non-existent, see Figure 1. Sweden recovers more energy from each ton of waste (3 MWh/ton) compared to other European countries [14] and in 2013 2.1 million tons of waste was imported to be utilized as an energy source, about 85% was Recycled Waste Wood (RWW) and MSW. Sweden has 34 waste combustion facilities which receive around six million tons of waste yearly, with high fractions of bio-based material such as wood and paper [14]. The combination of such fuels and facilities with carbon capture and storage opens up for the possibility for using the streams for achieving negative emissions, and could be an added advantage of utilizing thermochemical conversion systems for waste with high fractions of bio-based material [4, 5].

Two dominating technologies for waste incineration in Sweden is grate firing and fluidized beds [15]. When using fluidized bed boilers, two main types of ashes, bottom ashes (BA) and fly ashes (FA) are normally generated. These ashes contain considerable amount of metals, salts and other components some of which could be toxic, but in certain cases also have economic value. For example, heavy metals and compounds including Pb, Zn, Ni, Cu and Cr are extensively used by various metal-finishing, mining and chemical industries. High concentrations of these metals in ashes increase their toxicity and thereby handling cost, but it also prevents their use as fertilizers to soils and forests [16]. Since these metals are volatile and commonly end up in the FA, this ash fraction has been in focus for metal extraction, especially for Zn, Cu and Pb [17-20]. Most of the produced ashes are landfilled which is not a sustainable treatment option. Recently some new type of fluidized bed combustion systems has been proposed which uses oxygen carriers as bed material, e.g. Chemical Looping Combustion (CLC) and Oxygen Carrier Aided Combustion (OCAC) [21]. These concepts can have significant advantages with respect to emission control, as will be discussed below. By utilizing metal oxides in combustion processes, it is possible that the boiler chemistry is affected, which in its turn could alter the phase distribution of trace elements. The term trace elements refer to elements at concentrations below 0.1 wt% and may cover a large part of the periodic system. These elements occur naturally in the ecosystem and the concentration can vary largely, in part due to anthropogenic sources. A subclass of the trace elements are heavy metals, which include Cd, Pb, Hg, Zn and Cu for example. In waste fuels these elements can be present in such amounts that they could actually be minor (0.1-1.0 wt%) elements [22]. Therefore, in this thesis the term trace elements and heavy metals will be used interchangeably.

The interaction between different heavy metals and OCs is an unexplored field of research and the focus of this thesis is more specifically to study the fate of the trace elements Zn, Cu and Pb in the presence of oxygen carrier particles.

1.1. Waste Fuel Composition and Heavy Metals

A typical analysis of MSW can contain food waste, paper, plastics, wood, textiles, rubbers, leathers, cardboards, yard waste, shoes, batteries, shredder waste etc. [23]. In PVC plastics, heavy metals such as Ba, Cd, Pb and Zn are used in stabilizers while the use of Sb, Al and P is common in flame retardants. PVC plastic is also the main source of organically bound Cl while salt is the main source of inorganically bound Cl in MSW. Leather is prepared by chrome

tanning to create soft and formable leather. It involves preparations by soaking in chromium and sulfate solutions. This results in elevated levels of Cr and S in leather ashes. Shredder waste itself has many different constituents such as rubber, plastics, iron, glass and other materials. It may be enriched in metals such as Al, Cu, Cr, Ni, Pb and Zn [24]. Other sources of heavy metals in MSW could be due to common alkaline non-rechargeable batteries which typically include Cu wires, Zn anodes and traces of Hg, while rechargeable batteries may include Ni metal hydride, Li ion and Cd.

Recycled waste wood is comprised of different wood fractions originating from construction, demolition and refurbishment works. RWW is often the more economical option as the price is approximately half of those of wood chips. The composition of RWW may vary widely, especially regarding trace elements [16]. For example, compared to forest fuels, RWW may contain higher amounts of chlorine [25]. The main heavy metals originate from surface treatment, industrial preservative treatment, plastics and/or galvanization. For example, surface treated wood is the main source of Pb and Zn in pigments based on Pb chromate, Pb titanate or Zn oxides. Copper Chromated Arsenate (CCA) has been used as wood preservative which contain Cr, Cu, As and some S. However, in 2004 EU introduced restrictions against CCA which has lowered the amount of CCA-treated wood [26]. Substantial quantities of CCA have been used daily and for a long time and there are currently no EU directives stating that CCA-treated wood should be removed from their current applications. Therefore, it is expected to remain in use for some years to come.

The thirds waste fuel of interest for this thesis originated from end-of-life vehicles (ELVs). There are around 6 to 8 million ELVs in EU which generate around 7 to 8 million ton of waste yearly. ELVs are processed in three main phases: depollution, dismantling and shredding [27]. Around 75 wt % of a vehicle is ferrous scrap metals and materials which can be mechanically recycled. The remaining 25 %, which cannot be further separated or recycled is called Automotive Shredder Residue (ASR) corresponding to an amount of around 2 million tons yearly. Due to its heterogenous nature and complex composition ASR has been largely landfilled [27]. ASR consists of glass, fibers, rubbers, foams, wood, metals and a variety of plastics. The high metal content in ASR could consist of Fe, Al, Cu, Zn, Pb, Cr and Ni which affects the composition of the ashes and their disposal [28, 29]. Pb is commonly used as stabilizer in plastics, electronics and wires. Zn is used in applications involving casting, coating, door handles and locks while the major source of Cu is from the wiring and electrical components. The content of these elements in ASR-ash could reach levels around one weight percent.

The ash composition of wood fuels (chips, pellets), RWW, MSW and ASR is presented in Table 1. The table reports minimum and maximum values of the major and minor ash components. Note that imported fuels may vary in composition. For example, when comparing the metal concentrations of Swedish RWW and imported RWW it has been noted that the latter displays higher median concentrations of Pb, Hg and Cd while Swedish RWW contain higher concentrations of As, Cr, Cu, Ni and Zn [30].

Table 1. Composition[*] of common ash forming elements in waste and biomass fuels which are of interest for this thesis. Minimum and maximum values reported for major and minor ash components as wt% ash dry while trace elements are reported as mg/kg ash dry [25, 31, 32]. Papers refer to the appended articles in the thesis.

		Wood fuels		Recovered Waste Wood		Municipal Solid Waste		Automotive Shredder Residue	
Paper		II, IV		II		II-III		IV	
		Min	Max	Min	Max	Min	Max	Min	Max
Ca	wt% dry	9.9	26.2	4.5	12.4	11.9	16.5	6.3	6.7
Si		5.7	23.5	5.4	17.2	15.5	20.2	13	14
Al		0.4	4.2	0.8	3.3	4.2	10.9	4.5	5.1
Fe		0.9	2.5	0.9	6.0	2.3	3.7	22	23
Na		0.3	0.7	0.6	1.9	2.6	3.3	1.6	1.6
K		6.7	9.0	1.0	2.6	1.4	1.7	0.9	0.9
Cr	mg/kg dry	40	118	81	3 191	400	1 340	1 300	4 000
Cu		68	165	75	1 912	1 200	9 600	11 700	17 400
Sb		-	-	2.5	53	-	-	-	-
Ni		12	147	14	106	100	470	840	2 000
Pb		-	-	140	28 611	640	9 300	1 800	2 300
Zn		1 867	3 130	2 420	184 167	2 700	6 000	43 000	46 900

[*]According to standard SS-EN-ISO 18122:2015

2. Background

The flexibility, efficiency and stability of circulating fluidized bed (CFB) boilers is advantageous for biomass combustion. The ability to handle a wide range of fuels with different shapes and sizes allows heterogenous waste fuels to be utilized. There are several technologies which utilize fluidized beds for thermochemical processing of waste and biomass, and they will be further elaborated on below.

One of these is Chemical Looping Combustion (CLC). The main advantage with CLC is that CO_2 is obtained at high concentrations, which is suitable for CO_2-capturing. The basic principle of CLC is that fuel is oxidized/reduced using two separate reactors, called Air Reactor (AR) and Fuel Reactor (FR), as seen in Figure 2. Metal oxides (Me_xO_y), referred to as oxygen carriers (OC), transport oxygen between these two reactors. In the FR oxygen carriers are reduced (Me_xO_{y-1}) by the fuel according to reaction (1). The OCs are then transported to the AR where air is used to oxidize the particles according to reaction (2) before they are returned to the FR again.

$$(2n+m)\,Me_xO_y + C_nH_{2m} \rightarrow (2n+m)\,Me_xO_{y-1} + mH_2O + nCO_2 \quad (1)$$

$$Me_xO_{y-1} + \frac{1}{2}O_2 \rightarrow Me_xO_y \quad (2)$$

Another technology utilizing two reactors is Dual Fluidized Bed (DFB) gasification [33]. This process is based on thermochemical conversion of biomass to gas. DFB gasification consists of two reactors, a boiler and a gasifier, connected with loop seals. The bed material, usually silica or olivine sand, is circulated between the two reactors. The bed is heated in the boiler and thereafter transported to the fuel reactor. The fuel is first devolatilized, and the char is then gasified by H_2O and CO_2 according to reaction (3) and (4). With an excess amount of H_2O, H_2 will form through the water-gas-shift reaction (5).

$$C + H_2O \rightarrow \mathrm{CO} + H_2 \quad (3)$$

$$C + CO_2 \rightarrow 2\,\mathrm{CO} \quad (4)$$

$$CO + H_2O \leftrightarrow CO_2 + H_2 \quad (5)$$

Replacing the bed material with OCs will create a Chemical Looping Gasification (CLG) process [34]. This will allow the devolatilized and gasified products to partially be oxidized by the OC according to reaction (6) and (7) but also reaction (1). The OCs are thereafter circulated back to the boiler where they are oxidized according to reaction (2) and the process is repeated.

$$Me_xO_y + nH_2 \rightarrow Me_xO_{y-1} + \mathrm{n}H_2O \quad (6)$$

$$Me_xO_y + \mathrm{nCO} \rightarrow Me_xO_{y-1} + \mathrm{n}CO_2 \quad (7)$$

The outlet from the fuel reactor will ideally contain a mixture of CO, H_2, CO_2 and H_2O. One advantage with using oxygen carriers is that the combustion heat of DFB is "replaced" by the heat of oxidation in the air reactor, i.e. no fuel combustion is necessary in the air or combustion reactor. This would be an advantage if the process would be coupled to a carbon capture process, as all converted carbon is obtained in the concentrated stream from the fuel reactor.

A third use for oxygen carriers is during conventional combustion in CFB boilers. This technology is referred to as Oxygen Carrier Aided Combustion (OCAC) [21, 35, 36], see Figure 2. This is realized by replacing the commonly used inert material, such as silica sand, with OCs. This replacement has several advantages. The active bed material will be reduced in fuel rich parts and oxidized in oxygen rich parts, according to reactions (1) and (2), leading to an even oxygen availability and temperature in the boiler. Additionally, it can increase both combustion efficiency and capacity. It has also been shown that this replacement reduces risk for

agglomeration and has positive effects on emissions levels [37]. Since CFB boilers are used in industrial applications, OCAC can be a bridging technology towards CLC. The OCAC-concept has been successfully operated in industrial application where ilmenite has been used as a bed material [21, 36]. The main advantage with OCAC is that the technology can take advantage of existing CFB boilers. In recent years OCAC has been demonstrated at industrial scale, still the research around the technology is relatively limited [35, 36].

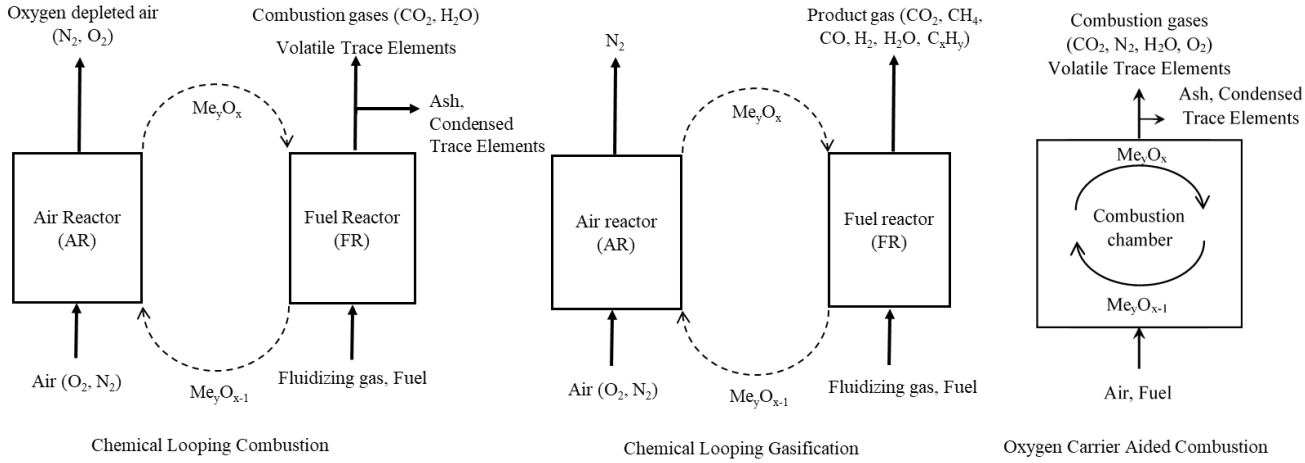

Figure 2. Schematic description of Chemical Looping Combustion (CLC) to the left, Chemical Looping Gasification (CLG) in the middle and Oxygen Carrier Aided Combustion (OCAC) to the right. All processes utilize metal oxides (Me_yO_x) as oxygen carrier.

2.1.Ash Interactions with Oxygen Carriers

A suitable OC should have low cost, have high oxygen transport capacity and selectivity towards CO_2 and H_2O but also be resistant to agglomeration and attrition. Many different OCs have been studied, both synthetic and natural ores, with different preparation methods and support materials. For example, iron-based oxygen carriers are both environmentally friendly and economically viable due to their abundance [38]. Furthermore, iron-based OCs have high melting temperatures which reduces the risk of agglomerations [39]. A disadvantage with using iron-based OCs is that they show comparably low oxygen transport capacity [40]. There are various iron ores that have shown favorable attributes as oxygen carriers and have been operated in CLC pilots [41, 42]. For example, ilmenite is an iron and titanium ore, which has been extensively examined as OC [43-46]. Ilmenite has good fluidization properties, high melting point, low production of fines and can be utilized without much pre-treatment. It has also been used as an OC in several commercial WtE units in Sweden, based on fluidized bed combustion and oxygen carrier aided combustion [36].

The oxygen carrier may interact with ash during combustion which can cause deactivation, agglomeration or attrition of the OC. The effect of different ashes will depend on ash content, mineralogy, experimental conditions and OC composition [47]. Agglomerations are usually caused by reaction of alkali with silica forming alkali silicates which have low melting temperatures [48, 49]. Gu et al found that K rich biomass ashes with relatively low amount of Si improved the reactivity of iron ores in CLC [50]. On the other hand, K and Si rich ashes produced molten potassium silicates causing particles sintering and reactivity deterioration [50]. Thus, ash components at the surface or in the bulk of the OC may alter the reaction kinetics. For example, the reaction rate can be decreased if gas diffusion is hindered by an ash layer formed on the surface of the particles. However, ash components on OC could also have a catalysing effect on the reaction or even have oxygen carrier properties itself [51] for example $CaSO_4$ [47].

While most studies with respect to OC and ash interactions mechanisms have been conducted on laboratory scale few studies are conducted at industrial scale. There are some limited research conducted on the ash layer build-up and S interaction when using ilmenite in OCAC-applications [52-54]. Ilmenite has been examined as oxygen-carrying bed material for OCAC, both at industrial and semi-industrial scale [21, 36]. When studying ilmenite particles that had been operated in a 12 MW_{th} CFB boiler with biomass as fuel, it was seen that a segregation of Fe to the surfaces and an enrichment of Ti in the particle core had taken place [53-55]. A Ca-rich double layer on the particle had also been formed, which surrounded the iron layer [54]. Both the separation of Ti and Fe as well as the Ca layer have been observed previously under CLC-conditions [43]. Other studies have found that with increased time of exposure, K migrates into the ilmenite particle core [54], and that depending on the chemical compound of K when interacting with ilmenite it will lead to different outcomes [56]. Before the start of this work, there were no studies conducted on the fate of trace metals with OCs. As some of these could be highly relevant with respect to corrosion and agglomeration issues in fluidized beds, in addition to being important with respect to ash characteristics, it was deemed important to study the fate of such species.

2.2.Trace Element Release – Effect of Ash Components

The volatilization behavior of trace elements is coupled to the availability of Cl in the gas phase. Since the affinity towards alkalis are higher compared to metals (H > K/Na > Pb > other heavy metals), alkalis will in its turn govern the availability of Cl [57]. When alkali and heavy metal chlorides form, they follow the flue gas into the convection path of the boiler where they can cause corrosion and fouling [58]. It has been reported that heavy metal chlorides can induce corrosion at temperatures as low as 250-300℃ [59] and the formation and behavior of heavy metal compounds are not yet as widely understood as alkali metals. The formation of gaseous alkali chlorides also promotes reaction with silicates due to increased mobility [48]. Thus, the alkali balance in the boiler is also affected by the interaction with the bed material. If other bed material than the common silica sand is used it may reduce the risk for agglomeration [60] however, it could lead to increased concentrations in the gas phase increasing the risks of deposition of alkali components downstream of the heat transfer surfaces. As the fuel resource base is expanding to include more waste fuels there has been more focus on heavy metal induced corrosion [61]. To summarize, the total amount of metals released to the gas phase is related to:

1. Fuel characteristics – Fuel composition, size, structure and residence time.
2. Combustion temperature – Higher combustion temperatures favor formation of gaseous species.
3. Reduction potential – More reducing condition will favour formation of gaseous species.
4. Chemical surrounding and sinks – Ash composition and type of bed material; oxygen carrier, silica sand etc…

The chemistry of trace elements in presence of OCs is an unexplored field, although the chemistry during normal combustion has been studied [62-64]. The complex behaviour of these elements may be associated with the intrinsic volatility of the species. One important model for transport of heavy metals during combustion is the so-called “volatilization condensation theory” which has been used to predict the location of elements in fly ash particles based on boiling points [65, 66]. Elements with boiling points above the typical combustion temperature are part of the core of the matrix while elements which evaporate during combustion be incorporated or deposited on the fly ash particle surface. Figure 3 shows the classification and volatility of relevant elements. Trace elements studied in this thesis are marked in red. The elements in Class IV are commonly emitted to the gas phase while the elements in Class III are

expected to evaporate and condense downstream of the combustion chamber. This condensation may lead to enrichment in smaller ash particles or aerosols. Class I elements are enriched in the bottom ash relative the fly ash and Class II elements are equally distributed between bottom and fly ash.

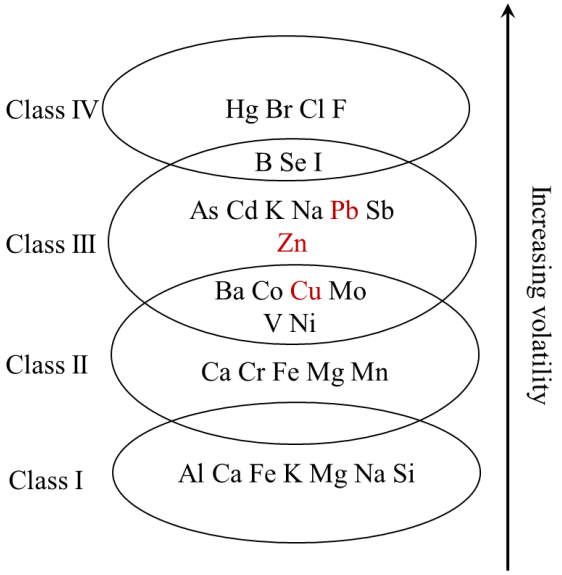

Figure 3. Classification of trace elements in combustion and gasification based on volatility, revised figure based on reference [67].

In systems utilizing OCs a complex chemistry can be expected with chemical transformation of metals in the gas-phase as well as interaction between bulk gas phase, ash components [62] and OCs. There are many possible reaction paths from when one element is released from the fuel before reaching and interacting with the OCs. The chemistry behind this will most likely depend on the volatility and activity, composition of surrounding gas phase and solid surface activity [68]. As observed in Figure 3 heavy elements such as (Pb, Zn, Cu, Sb, Ni) are concentrated in the fine ash fraction, the fly ash, which makes this ash fraction ecologically harmful. The total concentration of these metals in the ash provides limited information and to further evaluate the stability, knowledge regarding the oxidation state and interaction with other ash species and oxygen carrier is important.

2.3.Aim and Scope

The aim of this thesis is to study the interaction between the important trace elements copper, lead and zinc and oxygen carriers in different applications where oxygen carriers are present. A combination of theoretical and experimental methods has been used to gain knowledge about the fate of these elements, with specific focus on the heavy metal-oxygen carrier interactions. More specifically, this has been achieved by:

1) Development of a methodology to investigate the chemical speciation of trace elements after combustion of waste fuels in processes utilizing oxygen carriers.
2) Conducting detailed multiphase and multicomponent equilibrium calculations using combined databases.
3) Sampling of bed and fly ashes from several commercial units using waste fuels and oxygen carriers. Conducting detailed phase characterization of oxygen carrier and ashes using a variety of tools, including x-ray photoelectron spectroscopy.

It is believed that this integrated approach where thermodynamics and experimental phase characterization are combined provides a suitable workflow for studying trace element speciation in highly complex environments.

3. Theory and Methods

Laboratory scale experiments were conducted by isolating the effect of specific ash compounds on the interaction with OCs (**Paper I**). For the laboratory scale experiments synthesized ilmenite and hematite were used. The elemental content of these materials is presented in Table 2 [69]. Bottom ash samples investigated in this thesis have been obtained from two industrial plants utilizing OCAC (**Paper II-III**) and one semi-commercial DFB gasifier (**Paper IV**). The focus in this thesis has been mainly on the oxygen carrier ilmenite (**Paper I-III**). The experiments in **Paper IV** were conducted using olivine, which is not an oxygen carrier itself, but gained oxygen carrier properties due to the high metal content from the fuel ashes. The elemental content of the fresh ilmenite and olivine is presented in Table 2.

Table 2. List of investigated bed materials in this thesis. Reported compositions were provided by material supplier.

Sample		Hematite	Synthesized ilmenite	Fresh ilmenite	Fresh Olivine
Provider		Höganäs	-	Titania A/S	Sibelco Nordic
Unit	Paper	I	I	II-III	IV
Fe	wt% dry	75.5	40.8	33.3	6.8
Ti		0.01	24.8	23.9	0
Si		0.2		0.9	37.7
Ca		<0.1		0.3	<0.08
Mg		<0.1		1.8	46.9
Al		<0.1		0.3	0.3
Na		<0.05		0.1	<0.05
K		<0.1		0.1	<0.09
Mn		<0.004		0.1	0.1
Zn	mg/kg dry			100	28
Cu				100	2.9
Pb				<0.0001	<1

3.1. Laboratory Scale Experiments

In **Paper I** lab scale experiments were conducted to investigate the interaction between the oxygen carriers ilmenite and hematite and three different ash components potassium carbonate, calcium carbonate and silicon dioxide. As described above, K, Ca and Si can have significant implications for the ash chemistry, including trace element behaviour. By exposing the ash components together with OCs in oxidizing and reducing environments it is possible to investigate interactions which could be important in an AR or FR. The experiments were performed by mixing the oxygen carriers in 1:1 weight ratio of oxygen carrier to ash and 1:0.5:0.5 weight ratio of oxygen carrier to two ash components. The mixtures were exposed to oxidizing and reducing conditions in fixed-bed tubular furnaces together with tubular quartz reactors as presented in Figure 4. Both furnaces were manufactured by Vecstar, model VCTF4. Air was used for the oxidizing conditions and 2.5% H_2, 47.5% Ar and 50% H_2O was used for the reducing conditions, which may correspond reasonably well with the reducing potential which is present in a FR during CLC. When reducing conditions were used, the heat-up and the cool-down process were carried out in an inert atmosphere of nitrogen [70, 71]. The reduction potential, pH_2/pH_2O is 0.05 which corresponds to an equilibrium partial pressure of O_2 of $\log_{10}p(O_2)$ of -13.7 atm.

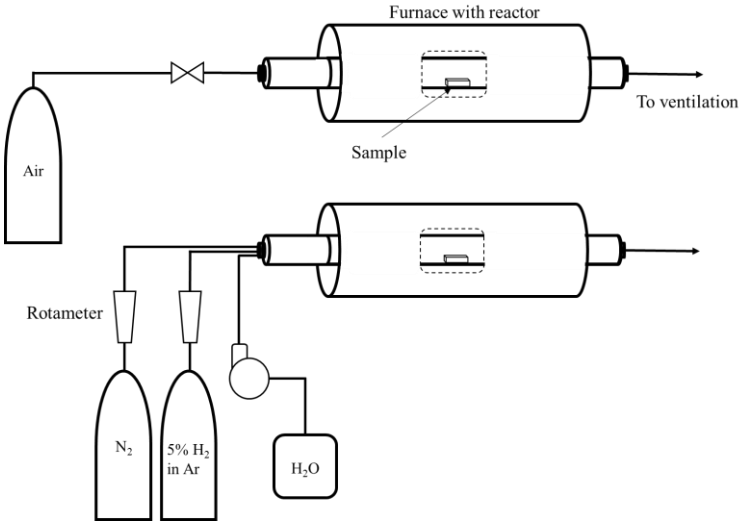

Figure 4. Schematic overview of the experimental system, ***Paper I****.*

The total flow through the reactors was 140 Nml/min. The air flow was controlled by a needle valve and the steam flow by a water pump (Watson Marlow 120U). A rotameter controlled the nitrogen and hydrogen in argon flow. All experiments were performed at atmospheric pressure. Before the exposures, the temperature profiles of the furnaces were determined with a thermocouple to know the exact position for the measured temperature. The furnace was heated to 900°C and the holding time was 6 h before the furnace was cooled down.

3.2.Semi-Industrial Scale

Chalmers Research Unit is a semi-commercial plant composed of a 10-12MW_{th} circulated fluidized bed boiler and 2-4MW_{th} bubbling bed gasifier. The layout and sampling points are presented in Figure 5. Bed material circulates between the gasifier (6) and boiler (2) via particle distributor (4) and two loop seals (5) and (7). As the unit has research purpose, the produced raw gas from the gasifier is not utilized as it would be in a commercial plant, but instead re-directed to the boiler where it is combusted [32]. The heat produced in the process is used for heating up Chalmers campus. Wood chips is the fuel fed to the boiler (1), which operates with a temperature above 850℃. The bed material is heated up in the boiler via exothermic combusting process and circulated to the gasifier where heat is released enabling endothermic gasification reaction of the fuel. The flue gases from the boiler pass through a cyclone (3) to remove fly ash. A secondary cyclone (9) removes finer particles before entering the textile filter (10). Lime is added before the textile filter (10).

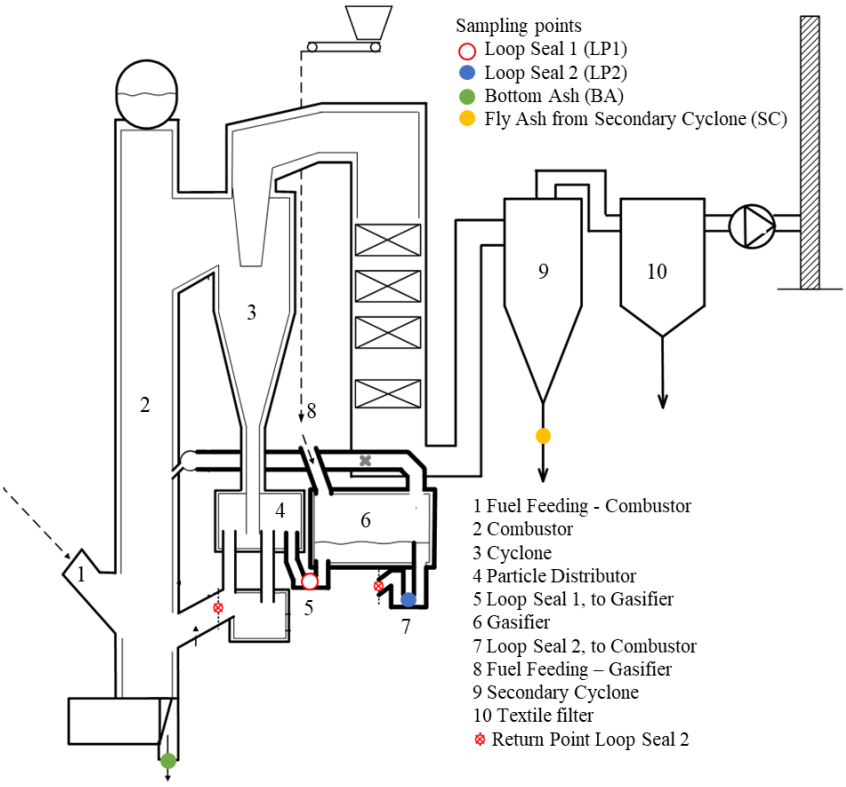

Figure 5. Illustration of Chalmers dual fluidized bed system. Sampling points are indicated in the figure. The red symbol represents the connection between loop seal 2 and return to the boiler, ***Paper IV****.*

During the experimental campaign, olivine sand was used as bed material, see Table 2. The gasifier was operated daily for 10 hours during weekdays for a total of 13 days, while the boiler was in continuous operation. Wood pellets were fed to the boiler and ASR to the gasifier. The olivine bed was replaced in small parts where addition and removal of the bed was made only to regulate the pressure in the boiler. Thus, ash was accumulated in the bed during the 13 days of operation. The ash originates mainly from ASR which is composed of 32-47 wt% ash, while ashes from wood pellets have significantly lower ash content, below 0.7 wt%. The ash contained significant amount of metals, Fe for example, meaning that the bed in fact obtained oxygen carrier properties, something which has been discussed by Pissot et al. [32].

3.3.Full-Industrial Scale

Ash sampling from industrial boilers provides unique opportunities to investigate the behavior of oxygen carriers under realistic conditions where complex fuels are utilized. In this thesis, samples from two such units have been characterized, and these are discussed more in detail below.

3.3.1. Kraftringen, Örtofta

The plant at Örtofta consist of a 115 MW_{th} CFB boiler which is owned by the company Kraftringen and has been in operation since March 2014. The plant supplies heat to the local heating grid by burning biomass. During operation around 60 ton of bed material is present in the system. Usually silica sand with an average particle size of 0.25 mm is used as a bed material but during sampling Norwegian rock ilmenite (**Paper II)** was used, see Table 2. The bed material, fly ash and flue gas enter one of the two cyclones at the top of the furnace. The cyclones separate the heavier particles from the flue gas, which falls to one of the two loop seals located at the bottom. The material is cooled by tertiary superheaters before being returned to the furnace. The boiler is equipped with a drum-sieve for bed material recovery which removes

larger fractions while the finer fraction, which is suitable as bed material, is recirculated back to the furnace. After the flue gases are cooled in the convection path the remaining particles are separated using textile filters. During the sampling period the fuel consisted of a mixture of recycled waste wood and wood chips. Further information can be found elsewhere [35].

3.3.2. E.ON, Händelö

The 75 MW_{th} CFB in Händelö is owned by the company E.ON. The plant provides heat to the local district heating network. Since November 2014 the boiler has been operating regularly with ilmenite (**Paper II-III**). In the boiler bed material is fed on top of the three fuel feeding ports. Through ports located at the bottom of the furnace coarse bed material is continuously removed, such as cables, metal parts, tiles, concrete etc. A drum sieve is used for bed material recovery where the recovered fraction is sent back to the boiler and the rejected fraction is sent to ash containers. Furthermore, a magnetic separator is located at the top of the boiler which separates the ilmenite rich magnetic fraction and recirculates the particles back to the boiler. At the top of the furnace two cyclones separate the heavy bed material from the flue gas, which falls to the loop seals located at the bottom of the cyclones. The material is cooled by tertiary superheaters before being returned to the furnace. During the period of these studies the temperature in the furnace varied between 880-935℃ respectively, and the outlet O_2-concentration was kept between 5-8 vol%.

The flue gas and fly ash which is not collected in the cyclone, continue through an empty duct where it is cooled from approximately 900℃ to 700℃ before reaching the superheater section and lastly the economizer. The temperature is lowered to approximately 170℃ after the economizer and the flue gas and fly ash enter the flue gas cleaning system, the Novel Integrated Desulfurization (NID) reactor. The cleaning process involves the use of limestone and activated carbon. It consists of a circulating system involving mixers, reactors, and textile filters. To begin with, activated carbon is injected into the stream after which the flue gases and fly ash reach the textile filters where remaining particles are removed. The cleaned flue gas goes through emission control before it is guided out through the chimney. After the textile filters the remaining fly ash is collected in the bottom and either sent to a silo or recirculated in the system. The recirculated fly ash is mixed with lime before entering the same flue gas stream, which is just before the addition of activated carbon and consequently the process is repeated. The boiler normally operates with MSW as base fuel but allows industrial waste, sewage sludge, rubber and demolition wood waste to be used as well. Detailed information can be found elsewhere [36].

3.4. Characterization Techniques

The total elemental composition of the sampled ashes was analysed using ICP-SMFS according to the standards EN ISO 17294-2: 2016 and EPA-method 200.8: 1994. This was performed by the external company ALS Scandinavia for **Paper II-III** and by RISE (Research Institute of Sweden) for **Paper IV**.

Information regarding the main crystalline phases were determined using powder X-Ray Diffraction (XRD) with $CuK_{\alpha 1}$ radiation in a Bruker D8 Advanced system. Bottom ash samples were lightly crushed in a mortar before analysed. Scans were made using the same settings (40kV, 40mA) over a 2θ-range between 20º and 80º with a step size of 0.05º and counting time 2s/step.

Morphology was examined using Scanning Electron Microscopy (SEM). The microscope is coupled to an Energy Dispersive X-ray spectroscopy (EDX) which allows study of elemental distribution within the particles. Samples were either mounted on carbon tape to investigate surface morphology or prepared by molding in epoxy resin. The molded samples were thereafter polished to study the cross-section of the particles. The system used for this

investigation was Quanta 200FEG coupled with an Oxford EDX system. Low-vacuum mode with charge reduction and back-scattered electron signals were used for imaging. For elemental distribution both point- and elemental map analyses were used.

X-ray Photoelectron Spectroscopy (XPS) was used as a surface material characterization which provides elemental and chemical state information for solid samples. Another strength with this method is the low detection limits which allows detection of elements down to 0.1 at%, something which is critical for the study of low-concentration trace metals. The PHI 5000 VersaProbe III Scanning XPS Microprobe (Base pressure of 1×10^{-9} bar) has been used with monochromated Al-source (25 W). Dual beam flood of low-energy electrons and low-energy argon ions were used to provide charge neutralization. Spectra was recorded with a 100 μm beam size and pass energy of 224 eV for surveys and 26 eV for region spectra. The survey spectra are used to quantify the surface composition while the region spectra, which record element specific regions, are used for chemical state identification. Several analyses were performed for each sample on different particles. Analysis points were chosen based on x-ray induced secondary electron imaging (SXI) allowing to specify points with good accuracy. The samples were either mounted on carbon tape to investigate surface features or molded in epoxy as to investigate the features inside the particles. Survey analyses were performed on at least three particles per sample, for both the cross section and surface. The metal concentrations reported in this thesis for both SEM-EDX and XPS are given in atomic percent. The given values are based on the ash elements and oxygen identified in each specific analysis.

Charge referencing was made to the adventitious C 1s line at 284.8 eV to calibrate the binding energies of other elements. The peak areas of each element were normalized by the atomic sensitivity factors (ASF) provided by Multipak software in the quantitative analyses of the surface composition [72]. Selected region spectra were recorded covering C1s, O1s, $Pb4f_{7/2}$, $Cu2p_{3/2}$ and $Zn2p_{3/2}$ for the chemical state identification [72, 73]. The region spectra were fitted using the Multipak software and a Smart background. Peak constraints regarding the area ratios and spin-orbit separation were defined as reported in literature [72].

3.5.Thermodynamic Equilibrium Calculations

3.5.1. Theoretical Background – Minimization of Gibbs Energy

The main equations and procedure for Thermodynamic Equilibrium Calculation (TEC) will be given below, applicable to the work in this thesis. For more detailed information the reader is referred to other sources, e.g. [74 , 75-77]. Thermodynamic equilibrium calculations (TECs) are used to determine the stable chemical and physical forms in a system. Data is stored in databases which include information on the standard reference state (T_{ref}=298.15 K, P_{ref} =1 bar) of enthalpy (H_f°) and entropy (S_f°), enthalpy change and temperature during phase transitions ($\Delta H_t, T_t$), and polynomial expressions of heat capacities ($c_p(T)$). These are then used to calculate the enthalpy (8) and entropy (9) at given temperature T.

$$H(T) = H_f^\circ + \int_{T_{ref}}^{T} c_p(T)dT + \sum \Delta H_t \tag{8}$$

$$S(T) = S_f^\circ + \int_{T_{ref}}^{T} \left(\frac{c_p(T)}{T}\right) dT + \sum \left(\frac{\Delta H_t}{T_t}\right) \tag{9}$$

Gibbs energy (G) is defined as equation (10) and can be calculated using the stored values from the databases, equation (8-9) [77].

$$G(T) = H(T) - TS(T) \tag{10}$$

In multiphase multicomponent systems, equilibrium at constant pressure and temperature occurs at a minimum of the Gibbs energy, and the minimization of G is performed under a mass balance constraint. The equilibrium condition is to minimize the Gibbs Energy in equation (11)

$$\mathrm{G} = \sum_{\Phi} \left(\sum_{i} n_i^{\Phi} \right) G_m^{\Phi} \tag{11}$$

where G_m^{Φ} is the molar Gibbs energy and n_i^{Φ} is the molar quantity of the phase constituent i in the phase Φ. The outer sum runs over all phases (Φ) and the inner sum over respective phase amount (n_i^{Φ}). Along with the equilibrium condition to minimize equation (11), mass balance (12) needs to be conserved.

$$\sum_{\Phi} \sum_{\mathrm{i}} n_i^{\Phi} a_{i,j}^{\Phi} = b_j \tag{12}$$

where n_i is the molar quantity of specie i, $a_{i,j}$ the stoichiometric coefficient and b_j molar quantity of component j. Furthermore, the Gibbs phase rule also needs to be satisfied. The Gibbs phase rule describes the number of components (C) and phases (P) which can be varied freely in a system. For example, the three variables in a chemical system is temperature, pressure, and chemical composition. In a multicomponent system the mole fractions in a phase can all be varied freely except for one since the sum must be equal to one. Thus, in one phase the composition is defined by (C-1) fraction terms. In total, this results in P(C-1)+2 number of variables, including two state variables that can be varied freely (temperature and pressure). Given that the system is in equilibrium the chemical potential μ_i^{Φ}, for a given chemical component must be equal in all coexisting phases. This results in total of C(P-1) number of constraints. The net number of degrees of freedom (F) is then determined by adding all variables and subtracting the number of thermodynamic constraints resulting in F= 2+P(C-1)-C(P-1)=2+C-P. This correlates the number of phases under equilibrium directly to the number of components.

Several methods can be used to minimize the Gibbs energy in multicomponent systems with the constrictions defined above [78, 79]. To minimize the Gibbs energy, the Lagrange method of undetermined multipliers can be applied. Minimization of the Lagrangian function L in equation (13) is equivalent to minimization of equation (11).

$$L(n, M) = G - M_j \left(\sum_{\Phi} \sum_{\mathrm{i}} n_i^{\Phi} a_{i,j}^{\Phi} - b_j \right) \tag{13}$$

where M_j is the Lagrange multiplier and $\mathrm{b_j}$ is the amount of $\mathrm{j^{th}}$ system component (often element). Consequently, a set of equations are derived according to equation (14).

$$\frac{\partial L(n, M)}{\partial n_i} = \left(\frac{\partial G}{\partial n_i} \right)_{T,P}^{\Phi} - \sum_{\Phi} \sum_{\mathrm{i}} a_{i,j}^{\Phi} M_j = 0 \tag{14}$$

The mass balance constraint may be represented by the matrix $\mathrm{a_{i,j}}$. To illustrate, a simple example describing the system ZnO–$\mathrm{Fe_2O_3}$ in air is used. The corresponding stoichiometric matrix $\mathrm{a_{i,j}}$ is presented in Table 3. Usually there are more species i than components j in a system.

Table 3. Example of the stoichiometric matrix $a_{i,j}$ for ZnO and Fe_2O_3 exposed in air.

Phase Φ	Constituents	Species i	Stoichiometric Coefficient $a_{i,j}$ of system components j			
			N	O	Zn	Fe
Gas	N_2	Gas_N_2	2			
	O_2	Gas_O_2		2		
	Zn	Gas_Zn			1	
	ZnO	Gas_ZnO		1	1	
Stoichiometric solids	Zn	Solid_Zn			1	
	ZnO	Solid_ZnO		1	1	
	Fe	Solid_Fe				1
	FeO	Solid_FeO		1		1
	Fe_2O_3	Solid_ Fe_2O_3		3		2
	Fe_3O_4	Solid_ Fe_3O_4		4		3
	$ZnFe_2O_4$	Solid_ $ZnFe_2O_4$		4	1	2

To calculate the equilibrium composition an iterative procedure can be used to obtain a set of molar quantities which yield the lowest value of the Gibbs energy while satisfying the mass balance constraint and the phase rule. For a given composition b_j, n_i^{Φ} and M_j need to be determined. This requires an initial estimation which is tuned in each iteration. At equilibrium the Lagrange multiplier M_j represent the chemical potential of the system components. It is evident from the matrix in Table 3 that the number of equations will increase when adding components, species and phases to the system. The numerical complexity is further increased when for example solid solutions are included. From equation (11) and (14) it is evident that expressions for the Gibbs energy is needed for each phase; stoichiometric, gas compounds and solutions. In the following sections different contributions and expressions for the Gibbs energy will be discussed.

3.5.1.1. Gibbs Energy for Stoichiometric Solids

Pure stoichiometric substances require the Gibbs energy $G_m^{\phi}(T,P)$ to be known as a function of T and P. Three different contributions may be distinguished and treated separately.

$$G_m^{stochiometric\ solids}(T,P) = G_{lattice}^{\phi} + G_{magnetic}^{\phi} + G_{pressure}^{\phi} \qquad (15)$$

1. The major contribution is expected to originate from $G_{lattice}^{\phi}$. This term depends on the database standard enthalpy of formation, standard entropy of formation and the heat capacity. The calculation of $G_{lattice}^{\phi}$ is performed by equation (10) which utilizes the stored data and combines equation (8-9).
2. $G_{magnetic}^{\phi}$ depends on the critical temperature (T_c) and magnetic moment (β). The lattice structure is considered in the function $f\left(\frac{T}{T_C}\right)$ which differs depending on if the temperature range is above or below the critical temperature.

$$G_{magnetic}^{\phi} = RTf\left(\frac{T}{T_C}\right) ln(\beta + 1) \qquad (16)$$

3. $G_{pressure}^{\phi}$ depends on standard molar volume (V^o), compressibility at 1 bar (K(T)) and thermal expansion (α(T)). Compressibility and thermal expansion coefficients are commonly expressed as polynomials. However, the pressure term is usually negligibly small and only a few substances have the relevant data available.

$$G^{\phi}_{pressure} = f(V^o, \propto(T), K(T), T) \quad (17)$$

3.5.1.2. Gibbs Energy for Gas Phase Components

The gas phase is often treated as ideal during calculations although it is possible to include virial coefficients and use the truncated virial equation of state (18) to treat real gases.

$$\frac{PV}{RT} = 1 + \frac{BP}{RT} \quad (18)$$

where B is estimated from the critical temperature T_c, critical pressure P_c and acentric factor ω. When treating an ideal gas, B is set to zero and minimization of the Gibbs energy is performed in order to determine the fraction of species in the gas phase. Thereafter the following expression is used to determine G_m^{gas}, where y_i represents the mole fraction among species.

$$G_m^{gas}(T,P) = \sum_i y_i G_i + RT \sum_i y_i ln y_i + RT ln P \quad (19)$$

3.5.1.3. Gibbs Energy for Solutions

While stoichiometric compounds require temperature and pressure, a solution also requires the quantity of each phase component $G_m^{\phi}(T,P,x_i)$ for example, solid solutions which have a range of compositions. Thus, for solution phases (ϕ) Gibbs energy consists of three contributions.

$$G_m^{\phi}(T,\mathrm{P},x_i) = G_m^{\phi,standard\ state} + G_m^{\phi,ideal} + G_m^{\phi,excess} \quad (20)$$

1. The properties of a solution are usually described relative the properties of the pure substance in the same structure and temperature. The first term in equation (20) is called the standard state term and contains the contribution of pure phase components. $G_m^{\phi,standard\ state} = \sum_i x_i G_i^{\phi}$ where x_i is the mole fraction of constituent i.
2. For an ideal solution the term $G_m^{\phi,ideal} = RT \sum_i x_i ln x_i$ is considered, which arise due to entropy of ideal mixing of constituents.
3. The non-ideal or so-called excess term needs to be described by some mathematical expression. This excess term is crucial for modelling eutectic mixtures or miscibility gaps for example. It is important that these equations consider different kind of bonds next to neighbors (AA, BB and AB). Data is often available for binary systems so these need to be extrapolated since information is scarce on higher order systems. FactSage includes different solution models, for example one and two-lattice polynomial [80], quasichemical [81] and Redlich-Kister/Muggianu. The complete set of available solution models can be found elsewhere [82]. Taking the one-lattice polynomial model as an example, random mixing of species is assumed (Bragg-Williams model) on a single lattice. The excess molar Gibbs energy is expressed as a polynomial (simple polynomial, Legendre polynomial or Redlich-Kister) in terms of site fractions. Then binary parameters are interpolated into ternary systems using either, Kohler, Toop, Muggianu or a combination of these techniques. To illustrate the complexity of the expression for the excess term, a restricted version of the one-lattice polynomial called Redlich-Kister/Muggianu is presented below. The Redlich-Kister/Muggianu polynomial for a solid solution with only one lattice site with random occupation is presented in equation (21). The interaction parameter, L_{ij} is often called interaction energy.

$$G_m^{\phi,excess} = \sum_i \sum_{<j} x_i x_j \sum_{v=0}^{n_{i,j}} L_{ij}^{v}(T)\left(x_i - x_j\right)^v + \frac{\sum_i \sum_{<j} \sum_{<k} x_i x_j x_k \left(x_i L_i^{ijk}(T) + x_j L_j^{ijk}(T) + x_k L_k^{ijk}(T)\right)}{x_i + x_j + x_k} \quad (21)$$

In this thesis the module *Equilib* in FactSage was used for all calculations. *Equilib* determines the combination of n_i^{Φ}, and x_i/y_i which minimizes the total Gibbs energy of the system at defined T and P including the gas phase, pure stoichiometric components, melts and solid solutions with data from selected databases. A flow sheet summarizing the procedure for multicomponent multiphase equilibrium calculations is presented Figure 6.

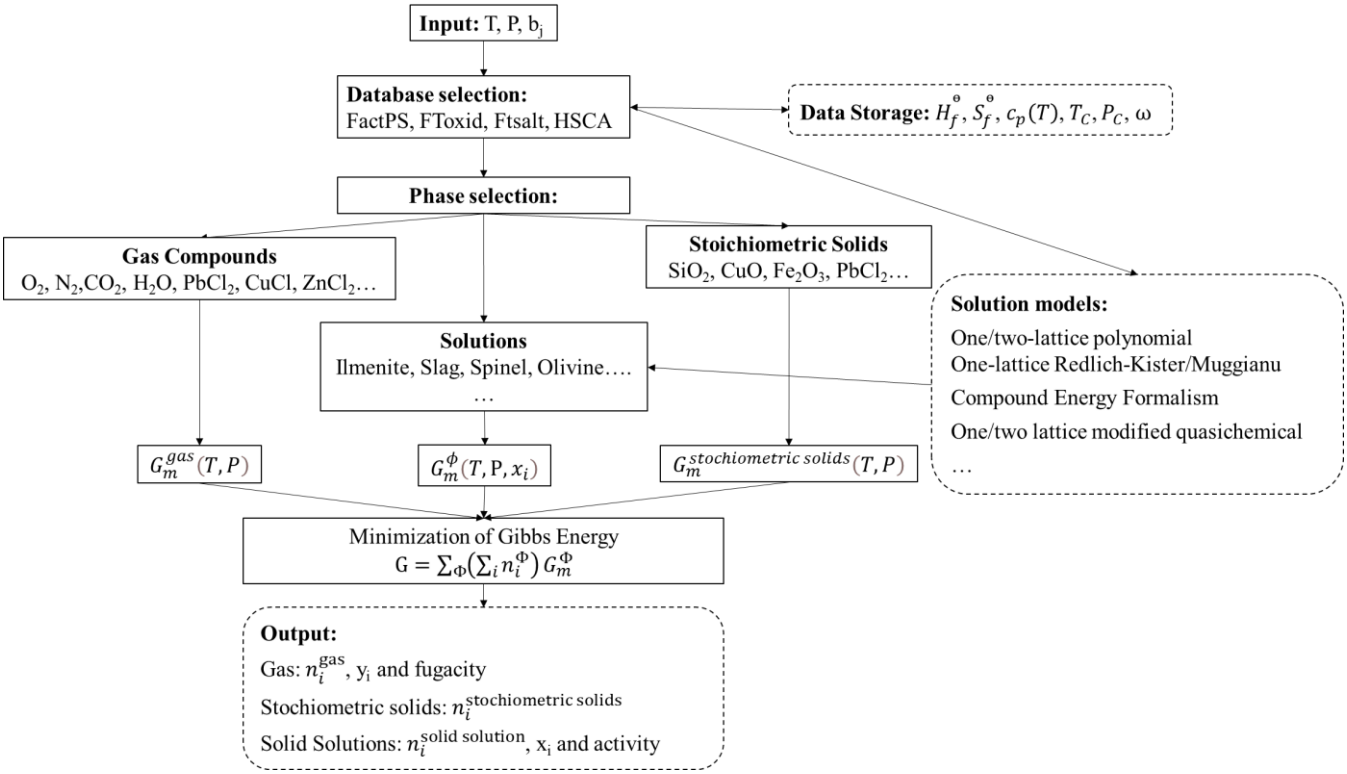

Figure 6. Schematic view of the calculation procedure in Equilib for multiphase multicomponent equilibrium calculations.

A summary of the solution phases and their major constituents in this thesis are presented in Table 4.

Table 4. List of phases used in this thesis along with their general formula, major constituents, and cation distribution.

Phases	General formula	Major constituents
Spinel	AB_2O_4	A = Al, $Co^{2+/3+}$,$Cr^{2+/3+}$,$Fe^{2+/3+}$,Mg, Ni^{2+}, Zn B = Al,$Co^{2+/3+}$,Cr^{3+},$Fe^{2+/3+}$,Mg, Ni, Zn + Vacancy
M2O3	A_2O_3	A = Fe, Al, Mn, Ti, Cr
Rutile		TiO_2
Titania_Spinel	AB_2O_4	A = Mg, Fe, Mn B = Mg, Fe, Mn, $Ti^{3+/4+}$, Al
Ilmenite	ABO_3	A = Fe^{2+}, Ti^{3+}, Mg, Mn B= $Ti^{3+/4+}$
Slag-liq		SiO_2 + (Na,K)AlO_2 + (Na_2, K_2, Cu_2, Ca, Mg, Pb, Zn)(O,S)
Olivine	$ABSiO_4$	A, B = Ca, Fe, Mg, Mn, Co, Ni, Zn
(Na)(Al,Fe)O2	SiO_2 + $ANaO_2$	A = Al, Fe
Wollastonite		$CaSiO_3$
Perovskite		$Ca_2Ti_2O_6$ - $Ca_2Ti_2O_5$
MgSO4-CaSO4(ss)		(Ca, Mg)SO_4
Salt-F	AB	A = Li, Na, K B = F, Cl, NO_3, SO_4, CO_3
Feldspar		(Na,K)$AlSi_3O_8$ - $CaAl_2Si_2O_8$
Nepheline		(Na,K)$AlSiO_4$, dissolving SiO_2 Ca and Fe
Clinopyroxene	$ABCSiO_6$	A = Ca, Fe^{2+}, Mg B = Mg, $Fe^{2+/3+}$, Al C = Al, Fe^{3+}, Si
Willemite	$ABSiO_4$	A, B = Zn, Fe^{2+}, Mg
Melilite	ABC_2O_7	A = Ca, Pb B = Mg, $Fe^{2+/3+}$, Al, Zn C = Al, $Fe^{2+/3+}$, Si

3.5.2. Thermodynamic Databases

As evident the results from thermodynamic calculations are dependent upon relevant and optimized databases. Amongst available thermodynamic databases are JANAF [83], IVTANTHERMO [84], SGTE [85], MTDATA [86], Thermo-Calc [87], HSC Chemistry [88] and FACT [76]. These vary considerably in terms of quality but also in terms of content. Thermodynamic equilibrium calculations are widely used to study the chemistry in combustion and gasification processes [89-92]. Early research by Frandsen et al. [89] investigated the fate of several trace elements in combustion and gasification of coal using a thermodynamic approach using the GFEDBASE database [93]. Later on data for Cd, Cr, Cu, As, and Pb was reviewed and compared for different databases by Lundholm et al. [94]. The number of compounds and thermodynamic data varied significantly, the variation was smaller for condensed phases and higher for gaseous species. Talonen, T. (2008) evaluated the data of twelve heavy metals (As, Cd, Co, Cr, Cu, Hg, Mn, Ni, Pb, Sb, Tl, and V) as well as Mo and Zn under both oxidizing and reducing conditions [95]. The difference between databases regarding heavy metal data was clear, HSC included 700 heavy metal species, the largest number, while FACT had 423 and JANAF only 150.

Recent research has focused on more heterogenous fuels such as waste and biomass fuels. A comprehensive review over available databases and models for waste and biomass combustion

have been presented by Lindberg et al. [96]. The authors concluded that there is no available thermodynamic database for the complete system (Na^+,K^+,Ca^{2+},Mg^{2+},Zn^{2+},Pb^{2+})/(CO_3^{2-},SO_4^{2-},S^{2-},O^{2-},Cl^-). However, the subsystem NaCl–KCl–$CaCl_2$–$MgCl_2$–$ZnCl_2$–$PbCl_2$ is available in the database FTsalt in FactSage where the thermodynamic properties of the system $ZnCl_2$ and $PbCl_2$ has been evaluated. The most comprehensive thermodynamic database is found in FToxid in FactSage for solid/liquid silicates and oxides of Al_2O_3, As_2O_3, B_2O_3, CaO, CoO, CrO, Cr_2O_3, Cu_2O, FeO, Fe_2O_3, GeO_2, K_2O, MgO, MnO, Na_2O, NiO, PbO, SiO_2, SnO, TiO_2, Ti_2O_3, ZnO and ZrO_2. However, no evaluation has been done on the ternary system K_2O–CaO–SiO_2 thus displaying some uncertainties. The introduction of $KAlO_2$/$NaAlO_2$ in the slag phase has showed to improve the accuracy of predictions of liquid properties [76]. Many authors have used the FactSage software to study ash interactions and trace element partitioning. For example, Becidan et al. [91] studied all separate waste fractions of MSW and their influence on the behavior of alkali metals and trace elements during combustion while Konttinen et al. [92] and Kramb et al. [97] studied the behavior of trace elements in fluidized beds and Enestam et al. [98] evaluated the condensation behavior of lead and zinc in bubbling fluidized bed combustion of recovered waste wood.

In this thesis the software FactSage will be used for thermodynamic calculations along with the databases FTsalt, FToxid and pure substance databases FactPS. As previously mentioned, HSC Chemistry has the largest number of available species with respect to the heavy metals. Therefore, relevant compounds were extracted from HSC to create a new database, here referred to as HSCA. More specifically, this database includes trace elements compounds of As, Co, Cr, Cu, Mn, Mo, Ni, Pb, V and Zn. Hence, it is believed that the quality of the calculations is improved with respect to these species. HSCA includes species originating from HSC Chemistry 9 **(Paper II, IV)** and HSC Chemistry 10 **(Paper III)**. Species which have been added to the HSCA-database are summarized in Appendix I.

3.5.3. Global and Local Thermodynamic Equilibrium Calculations

Both global and local multicomponent equilibrium calculations were performed using FactSage 7.2. Global equilibrium calculations were used to predict phase formation, phase distribution and effect of parameter variation to study the interaction between ash components and oxygen carriers. These calculations used elemental analyses of the three major components as input i) fuel composition, ii) bed material and iii) fluidizing gas (**Paper II-IV**). Local thermodynamic equilibrium calculations were based on the outermost surface composition as obtained from X-Ray Photoelectron Spectroscopy (XPS) (**Paper II-IV**). Local calculations are performed on specific particles to study the outermost surface as this is the area is in direct contact with the surrounding gas phase. The calculation output provides the equilibrium composition of gaseous, stoichiometric and solution components. Figure 7 illustrates the methodology for the two types of calculations.

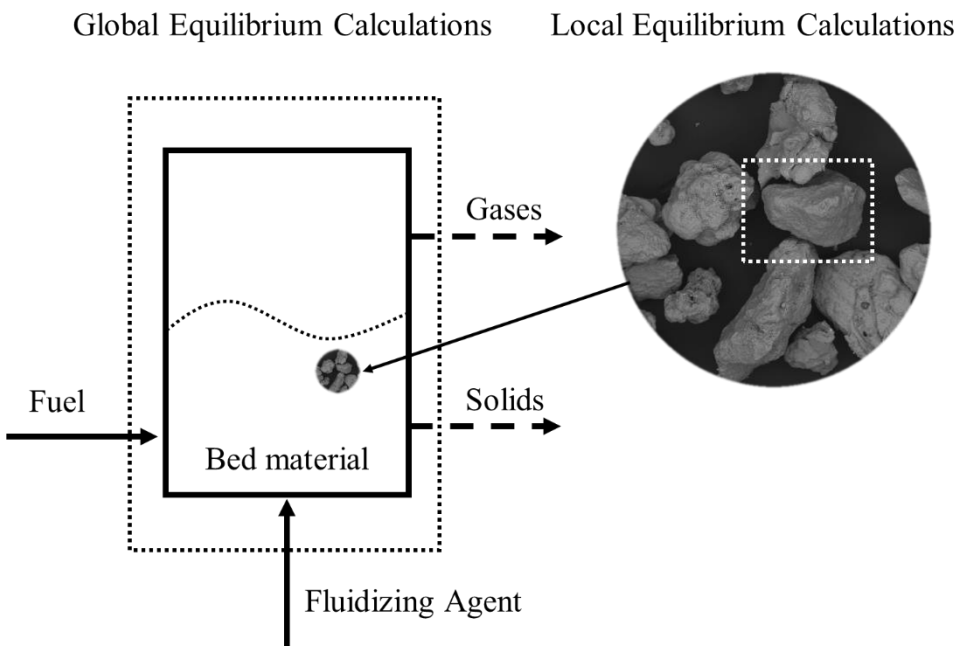

Figure 7. Description of the fluidized bed and clarification of the methodology for global and local thermodynamic calculations. Solid arrows represent the input and dashed arrows represent the output.

One of the parameters investigated in this thesis is the reduction potential, as it is expected that this could vary in the furnace and have implications for TE speciation. In **Paper II-IV** the phase distribution was studied over a range of oxygen potentials, expressed as the logarithmic oxygen partial pressure (pO_2) or reduction potential (pCO/pCO_2). Higher reduction potentials represent conditions further into the particle or for example oxygen deficient parts of a boiler. Table 5 summarizes the relation between these variables at 850°C. The corresponding air ratio, which relates the actual air supplied to the theoretical air required for complete combustion, is also included in the table.

Table 5. The relation between the logarithmic reduction potential, logarithmic oxygen partial pressure, air ratio and the yield of CO_2 at 850°C.

Reduction potential	Oxygen partial pressure	Air ratio	CO_2 yield
$\log_{10}[pCO/pCO_2]$	$\log_{10}[pO_2]$	$\frac{Air_{supplied}}{Air_{theoretical}}$	$\frac{pCO_2}{pCO + pCO_2}$
-8.0	-1.2	1.39	>0.9999
-7.9	-1.3	1.29	
-6.4	-4.5	0.97	
-5.0	-7.2	0.97	
-4.5	-8.2	0.96	$0.9999>\frac{pCO_2}{pCO+pCO_2}>0.9990$
-3.0	-11.2	0.96	
-1.9	-13.5	0.95	0.986
-1.1	-15.1	0.89	0.920
-0.6	-16.0	0.80	0.802
0.1	-17.5	0.48	0.420

4. Results

The results from the papers included will be presented in this section and cover both thermodynamic and experimental findings regarding the interaction between the metals Zn, Cu and Pb and OCs. The results are divided into the following three main topics, for more detailed information please see the paper in question.

- Evaluation of the interaction between OCs and alkali, alkaline earth and SiO_2. (**Paper I**)
- Chemical speciation of TEs during OCAC of waste:
  - Surface interaction between TEs and ilmenite particles. (**Paper II**)
    - Distribution of TEs in the cross section of ilmenite samples (**Paper III**)
- Chemical speciation during CLG of ASR. Surface speciation and distribution of TEs and olivine. (**Paper IV**)
- Comparison of phase prediction by TEC and detected phases by XRD (**Paper I-IV**)
  - Influence of temperature, reduction potential, chemical addition and bed material (**Paper III**)

4.1. Interaction of Oxygen Carriers with $CaCO_3$, K_2CO_3 and SiO_2

Lab scale experiments were conducted to investigate the interaction between the oxygen carriers ilmenite, hematite and hausmannite and three different ash components in their oxide state, potassium carbonate, calcium carbonate and silicon dioxide (**Paper I**). Of special interest for the work in this thesis is the chemistry of these components with ilmenite. Furthermore, alkali contents in the bottom ashes studied in this thesis reach levels up to 2 and 4 wt% dry (Na and K respectively). RWW ashes contain higher concentrations of K, while MSW ashes are enriched in Na. Although the ash chemistry of these components can be important in their own, they also play a valuable role in the behaviour of the trace elements.

The lab scale experiments show that ilmenite does not form new crystalline phases with either silica sand, calcium carbonate or a combination of these after six hours of exposure. On the other hand, exposure with potassium carbonate forms potassium titanates and potassium iron oxide. In the experiment with potassium carbonate and silica sand; potassium silicates formed, and melts were observed. Thus, mixing ilmenite with silica sand will provide two interaction possibilities for K where both potassium silicates and titanates can form. The former, is however, usually not desirable due to low melting points which could induce slag formation and possibly defluidization. Chemical mapping on the particle cross section using SEM-EDX reveal melt formation after exposure with ilmenite, K_2CO_3 and SiO_2. Exposures with K_2CO_3, with and without SiO_2, showed that potassium penetrated the ilmenite particle. Cross section micrographs are presented in Figure 8. This interaction was observed after both oxidizing and reducing experiments.

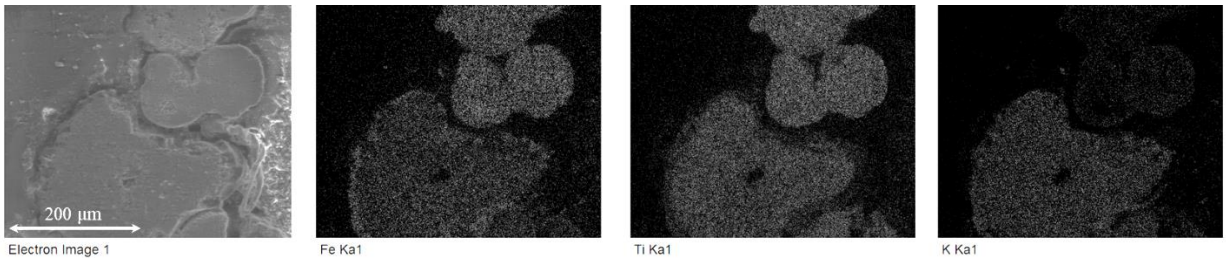

Figure 8. SEM micrograph and EDX intensity mapping of cross-section of ilmenite particles exposed with K_2CO_3 after oxidizing conditions.

Hematite interacted with calcium forming $Ca_xFe_yO_z$ in presence and absence of SiO_2. Exposure with potassium formed K_xFeO_y which was accompanied by sever agglomeration, both with and

without SiO_2. Capturing alkalis in the bed material could promote volatilization of heavy metals since the chemistry between chlorine, alkali and heavy metals is closely coupled. Cl is known to promote heavy metal chlorides, but the affinity is higher towards alkalis than heavy metals. Having a bed where alkali metals are accumulated in a solid lattice will allow more TEs to be associated with Cl. This will have implications on the samples obtained from full-scale experiments, and hence this study provided a valuable insight for the work with ilmenite and trace heavy metals.

4.2.Characterization of Bottom Ash Samples

The following section will elaborate on the interactions observed in semi- and full industrial scale operation. Elemental analyses of selected bottom ashes utilizing various waste fuels and bed materials, which were analyzed in this work are presented in Table 6. The table states type of sample, fuel, application, magnetic fraction (when applicable) and time with ilmenite feeding.

Table 6. Elemental analysis of selected bottom ashes analyzed in this thesis.

Sample		Ilmenite	Ilmenite	Ilmenite	Sand	Ilmenite	Ilmenite	Ilmenite	Olivine
Fuel		RWW	RWW	MSW	MSW	MSW	MSW	MSW	ASR
Magnetic		-	-	Yes	Yes	Yes	No	Yes	-
Application		OCAC	OCAC	OCAC	FBC	OCAC	OCAC	OCAC	CLG
Magnetic fraction [wt%]		70%	25%	26%	9.6%	19.6%	19.6%	41.6%	-
Time with ilmenite feeding		200h	505h*	100h	0h	550h	550h	893h	ǂ
Unit	Paper	II	II	II	III×	III×	III×	III×	IV
wt% dry	Fe	19.0	2.1	16.2	11.0	22.5	1.3	23.3	7.7
	Ti	16.0	1.6	9.3	1.5	7.0	0.7	12.8	0.4
	Si	4.8	25.7	9.6	16.6	8.6	31.9	7.4	18.0
	Ca	10.8	8.2	9.0	15.6	13.0	9.6	10.8	7.3
	Mg	2.0	1.1	1.6	1.8	1.4	0.8	1.9	19.0
	Al	1.5	3.0	2.5	4.7	2.6	4.2	2.2	1.6
	Na	1.0	1.3	1.2	2.0	1.0	1.6	1.1	0.6
	K	1.8	4.3	0.5	0.9	0.4	1.1	0.4	1.8
	Mn	0.6	0.5	0.2	0.2	0.3	0.1	0.3	0.5
	S	0.7	0.2	0.9	2.7	1.3	0.7	1.4	0.2
mg/kg dry	Cl	26	17	500	-	-	-	-	<100
	Cr	883	203	677	2 050	2 590	299	1040	650
	Pb	675	544	686	530	716	716	668	420
	Cu	810	702	3 180	2 390	6 310	6 020	5 210	3 400
	Zn	10 100	10 400	8 650	7 050	12 700	4 280	11 200	14 600

*200h after the start of silica sand feeding
× A time series available over 893h and a magnetic fraction between 11.2-44.7 wt%
ǂ Sample obtained from the bottom of the boiler after 13 days of CLG with ASR

In **Paper II** a detailed surface analysis was performed on ilmenite particles obtained after OCAC of MSW and RWW fuels. Composition of these three ashes is presented in Table 6. Since the boilers regularly operate with silica sand, sand samples were obtained for reference. The RWW reference sample is obtained 200h after silica sand was fed back to the boiler and as is evident from the table is that the ilmenite content, Fe and Ti, is relatively low. This study was followed-up in a more detailed investigation of the trace element distribution throughout the particles and the time influence during OCAC of MSW appended in **Paper III**. In this paper a time series of samples were obtained over a period of 893h. Magnetic separation was performed on these bottom ashes to obtain an ilmenite rich fraction. The corresponding magnetic fraction for each sample is presented in Table 6. MSW-Sand is obtained before ilmenite feeding started,

as reference, suggesting that the magnetic fraction lies around 9.6 wt% even without OC present, **Paper III.** The composition of the magnetic accepted and rejected fraction obtained after 540h with OCAC of MSW is also presented in the table. The elemental analysis of the two ash fractions show that magnetic fraction is enriched in Fe and Ti while the non-magnetic fraction is enriched in Si, which is expected.

In **Paper IV** the distribution of trace elements was investigated during CLG of ASR using olivine and the metal rich ashes as oxygen carrier. Samples were extracted from the bottom of the Chalmers boiler after 13 days of operation during which there was almost no replacement of the bed material. Table 6 shows that the ASR and RWW-samples, especially the Si rich RWW-sample, contain the highest amount of K while MSW-samples are enriched in Na. The non-magnetic MSW-sample contain slightly higher concentration of K compared with the magnetic fraction. Variation in trace element concentration can also be observed in the table where the olivine bed contains the highest concentration of Zn while the bottom ashes from OCAC with MSW contains the highest concentrations of Cu, Pb and Cr. Evident from the table is that the concentration of Zn and Cr are almost three and five times higher respectively, in the magnetic fraction of MSW-Ilmenite, compared with the corresponding non-magnetic fraction.

4.3.Interaction with Recycled Waste Wood

Similar to laboratory scale experiments (**Paper I**) chemical mapping and point analyses of the cross section of RWW-ilmenite particles show that small amount of K and Na is present inside the particles. However, in contrast to the lab scale experiments the cross-section analysis reveal interaction between Ca and ilmenite. As the particles undergo continuous redox reactions Ca migrates into the particle, see Figure 9. Under oxidizing conditions Fe will migrate towards the surface where the oxygen partial pressure is high, something which was observed in the laboratory experiments, Figure 8. A line scan over the ash layer is presented in Figure 9. It is observed that the ash layer contains Si, Mg, Ca and some amount of Na, K and Zn. Surface speciation by XPS of ilmenite particles showed that the major components at the surface are the ash elements Ca, Mg, Si, Al, S and Na (>5 at%) besides the OC elements Fe and Ti (**Paper II**).

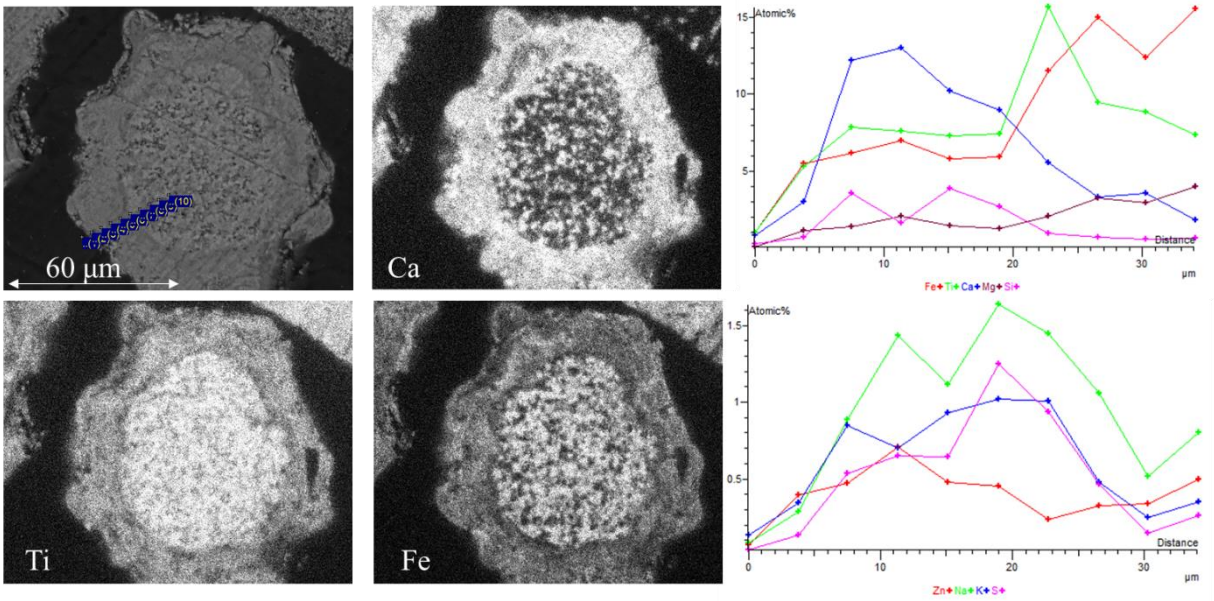

Figure 9. SEM micrograph of the cross section of sample obtained after 200h of OCAC of RWW with corresponding EDX intensity maps showing the elemental distribution. Chemical composition over the ash layer was acquired with line scan.

It is observed in Figure 9 that the Zn-content is enhanced in the ash layer following the same trend as Fe. The concentration is higher in the outer part of the ash layer. XPS confirmed the Zn content at the particle surface (0.6 at%) and the obtained binding energy from XPS region spectra point to the formation of $ZnFe_2O_4$. Cu was not observed in the surface intensity mapping or by XPS, however possible interaction should not be disregarded as fuel variations may occur. Pb which could not be observed in the surface micrographs, was successfully identified using XPS (0.1 at%). XPS region spectra showed that Pb is likely in the form of lead titanate.

4.4.Interaction with Municipal Solid Waste

Chemical mapping of the cross section of MSW-Ilmenite is presented in Figure 10 along with a line scan over the ash layer. Compared with RWW-ilmenite the ash layer is thicker and the composition of the layer is slightly different. The amount of K is much lower inside the MSW-ilmenite particles compared with RWW-ilmenite. Since the MSW-ilmenite bed is mixed with silica sand the availability of silica sand is high and potassium silicates also form. The K-concentration is slightly higher in the magnetic reject fraction, see Table 6. The content of Ca, Si and S is higher in the outer ash layer compared with Figure 9. An inner ash layer can be distinguished with the increased Fe-content. Surface speciation by XPS of ilmenite particles showed that the major components at the surface are the ash elements Ca, Si, Al, S and Na and that the concentrations of Fe and Ti were lower compared with RWW-ilmenite (**Paper II-III**).

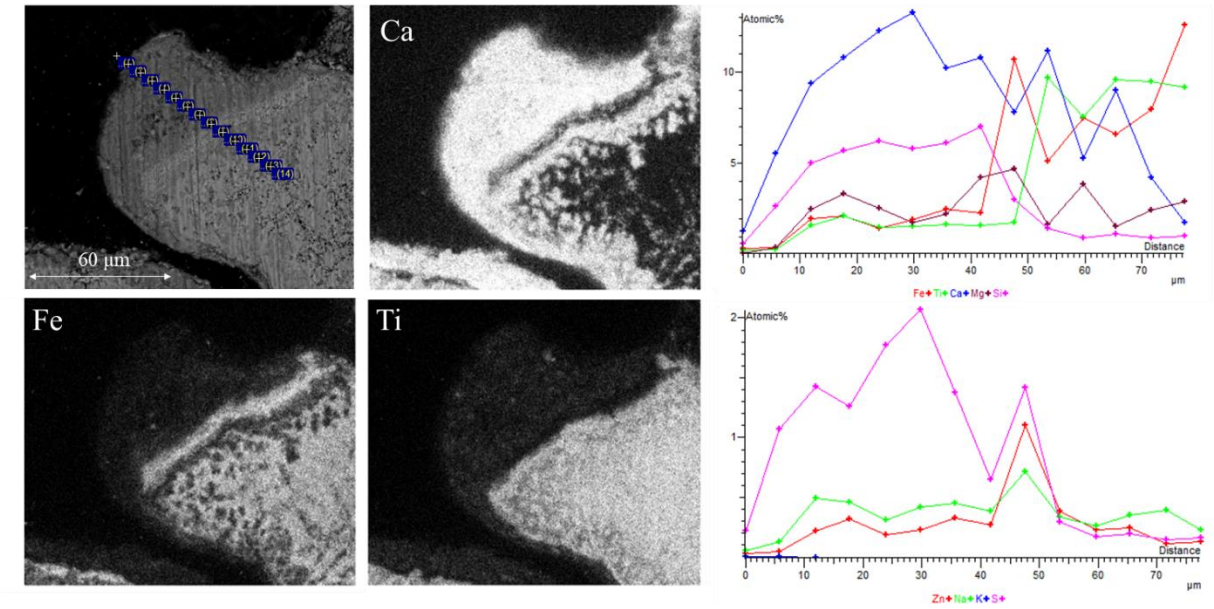

Figure 10. SEM micrograph of the cross section of sample obtained after three days of OCAC of MSW with corresponding EDX intensity maps showing the elemental distribution. Chemical composition over the ash layer acquired with line scan.

Once again it is observed that the Zn-content follows the Fe-content, Figure 10. The line scan shows that Zn is enriched in this inner Fe-rich layer. XPS region spectra identified Zn ferrites on ilmenite particles. The Cu concentration is noticeably higher for MSW ash, as seen in Table 6, which also allowed identification of copper ferrites on the particle surfaces. Pb, which could not be observed in the surface micrographs was successfully identified using XPS, however at low concentrations (0.1 at%) in the form of lead chlorides, titanates or silicates (**Paper II-III)**. The corresponding fly ashes were analyzed by SEM-EDX, which indicated formation of lead chlorides. Furthermore, larger bright spots of Cu and Zn could be correlated to enhanced intensities of Al or Fe while smaller spots were related to Cl. Formation of lead chlorides, zinc aluminates and ferrites, and copper ferrites and chlorides were confirmed during the XPS analysis. For further details, see **Paper II-III**.

4.4.1. Study of a Time Series

Trace element distribution throughout the particles were studied by XRD, SEM-EDX and XPS of a time series of MSW-ilmenite samples (**Paper III**). The influence of time and accumulation of ash elements on the particles was investigated**.** The surface and cross section concentration of Zn and Cu over a period of 38 days, as determined by XPS, is presented in Figure 11. The zinc concentration on the particle surface was detected up to 0.72 at% and the mean value lies in the range of 0.33-0.46 at% across the whole time interval. EDX intensity mapping and line scan reveal that Zn is incorporated in the Fe rich ash layer surrounding the double calcium layer. Two cross section Zn values slightly above 0.4 at% were detected with XPS. Based on the EDX elemental mapping, the concentration and chemical speciation ($ZnFe_2O_4$) it is likely that the interior Zn most likely originates from this Fe-rich ash layer.

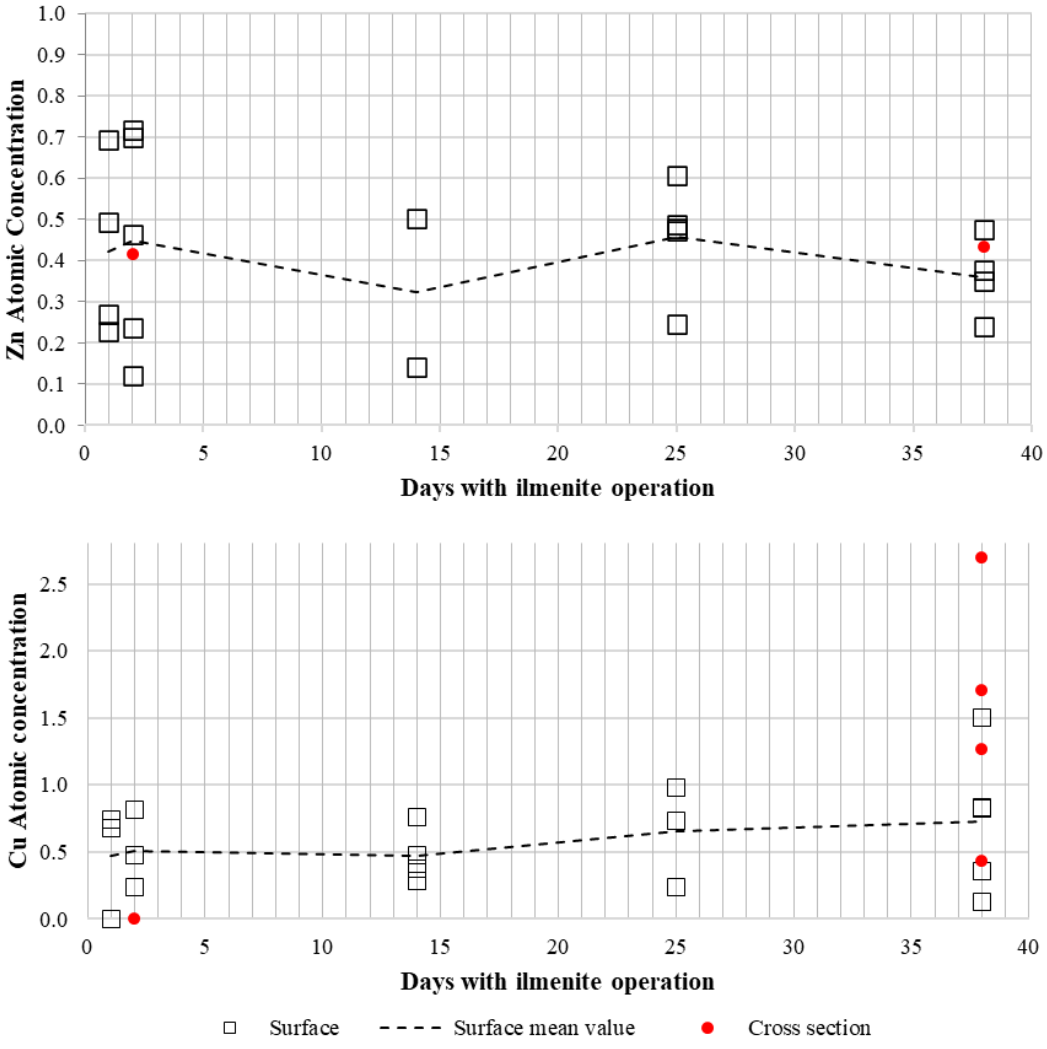

Figure 11. The atomic concentrations (at%) of zinc (top figure) and copper (lower figure) over time. Hollow squares indicate values on particle surface and solid circles indicate interior values. The dashed line presents the mean value of the surface concentrations as determined from XPS analysis.

Pb was more difficult to observe with SEM due to low concentrations. However, XPS identified the Pb surface content but the concentration never exceeded 0.1 at%. Both lead chlorides, titanates and silicates were observed on the particle surfaces over the period of 38 days. Pb was also detected in the particle interior by XPS and the corresponding binding energy is well aligned with lead titanate.

In Figure 11 one may observe that the cross-section concentration of Cu increases from day 2 to 38, indicating accumulation of Cu over time. The mean surface concentration lies in the range of 0.47-0.73 at% and seems to increase over time. XPS region spectra of the cross section revealed Cu^{+}, which is most likely in the form of $Cu_2Fe_2O_4$. This is in accordance with the detailed SEM-EDX chemical mapping in Figure 12 where Cu coexists with Fe. In the figure one can also observe coexistence of Ca and Ti while Fe is enhanced in small cracks and pores. Cu is observed to be concentrated in vicinity of these Fe-rich areas. Furthermore, the oxygen availability may be lower inside the particles and higher reduction potentials favor formation of $Cu_2Fe_2O_4$.

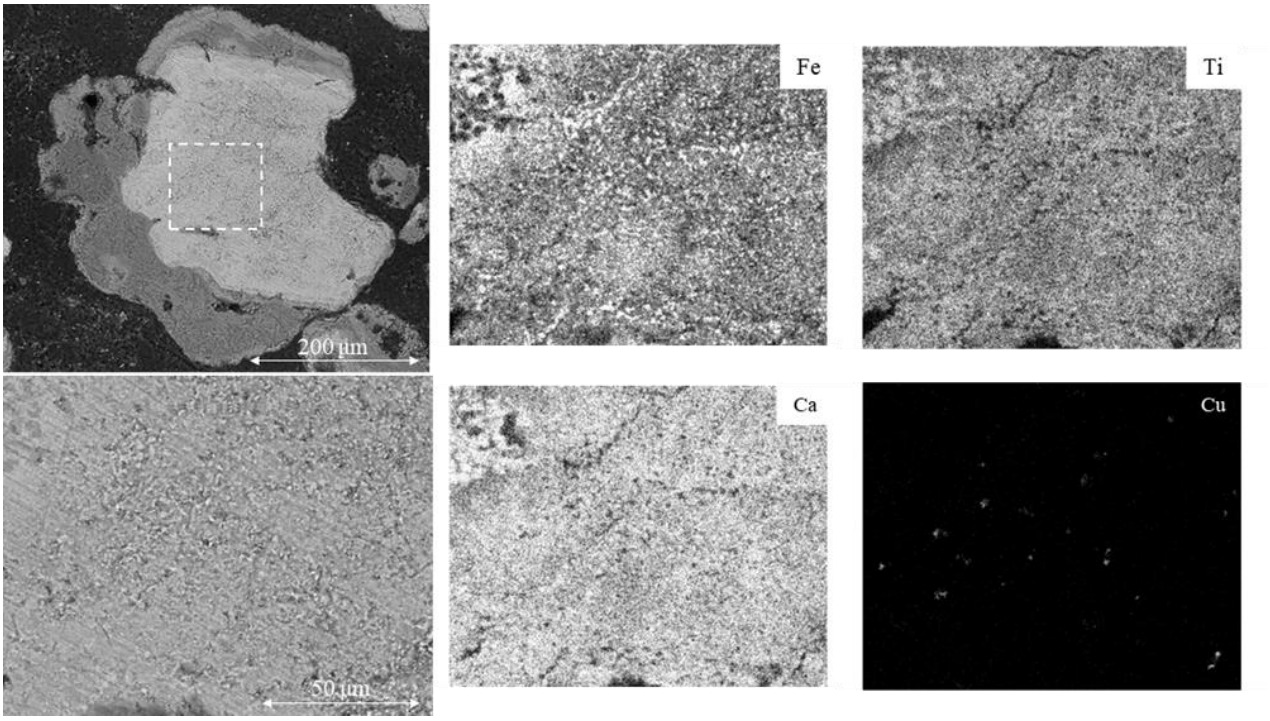

Figure 12. SEM micrograph of the cross section of an ilmenite particle obtained after 24 days of OCAC with MSW along with EDX intensity maps of Fe, Ti, Ca and Cu.

4.5.Interaction with Automotive Shredder Residue

The distribution of trace elements during CLG of ASR using olivine and the metal rich ashes as OC was investigated in **Paper IV**. The bed material originally consisted of olivine, which is not an oxygen carrier itself however, with increased time of exposure in the boiler the accumulation of the metal rich ASR ashes created an oxygen carrying bed material. Elemental analyses of the ash for different days indicate that the amount of Fe, Zn and Cu increase in the bed, which is predicted in the form of a ferrites by thermodynamic calculations. SEM-EDX surface micrographs of olivine particles show Fe-rich spots on the surface, Figure 13. An enrichment of Fe can be expected to form both from migration of Fe from inside the olivine particle to the surface [99] but also from Fe from the fuel ashes. It is also observed that the particles are covered in Ca and Si. The major surface components are Ca, Mg, Si, Fe, Na with some Al, K and S, **Paper IV**. The concentration of Cu and Zn are enhanced in these Fe-rich spots.

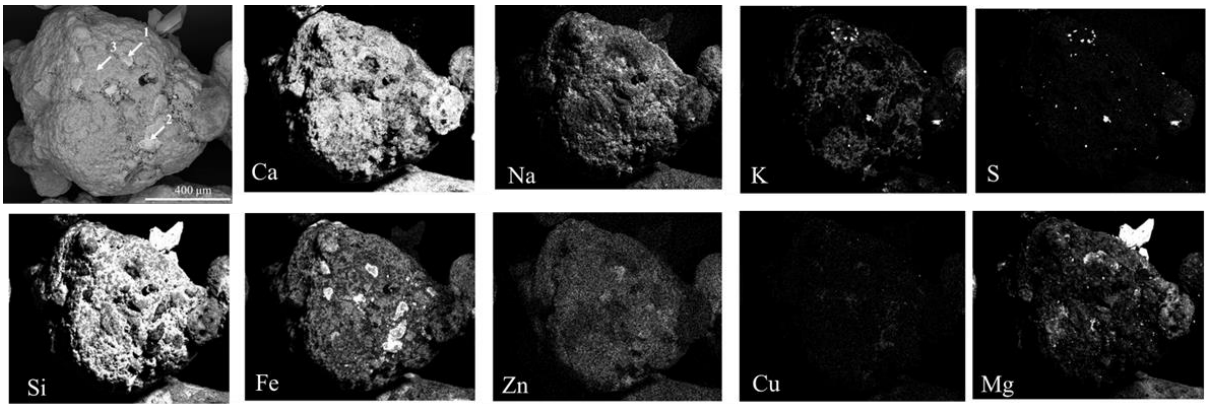

Position [at %]	Na	Mg	Al	Si	P	S	K	Ca	Ti	Cr	Mn	Fe	**Cu**	**Zn**
1	8.7	13.6	4.7	8.3	3	0.9	2.1	7.1	0.7	5.9	0.8	34.8	1.2	8.4
2	4.6	15.9	1.6	2.3	0	0.6	0.6	1.5	0.2	0	1.2	63.7	4.7	3.1
3	6.3	10.1	8.8	29.6	1.2	0.4	4.4	21.9	1.6	0	0.6	11.9	0.5	2.6

Figure 13. Top view SEM micrograph of a particle from the bottom ash after 13 days of CLG with ASR along with EDX intensity maps and point analyses in the indicated areas.

SEM-EDX analysis is presented in Figure 14 showing the cross section of the ash layer of an olivine particle. The formation of a Ca layer, previously described in olivine compounds, can be observed in the intensity mappings [100]. Fe is observed inside the particle, but with higher intensity at the surface. The intensity mappings do not indicate accumulation inside the particle of either Zn or Cu after 13 days of CLG. However, the intensity of Zn and Cu seem to be enhanced at the particle surface. A line scan over the particle surface shows that Zn is slightly concentrated in the outer ash layer (points 4-7, indicated in Figure 14).

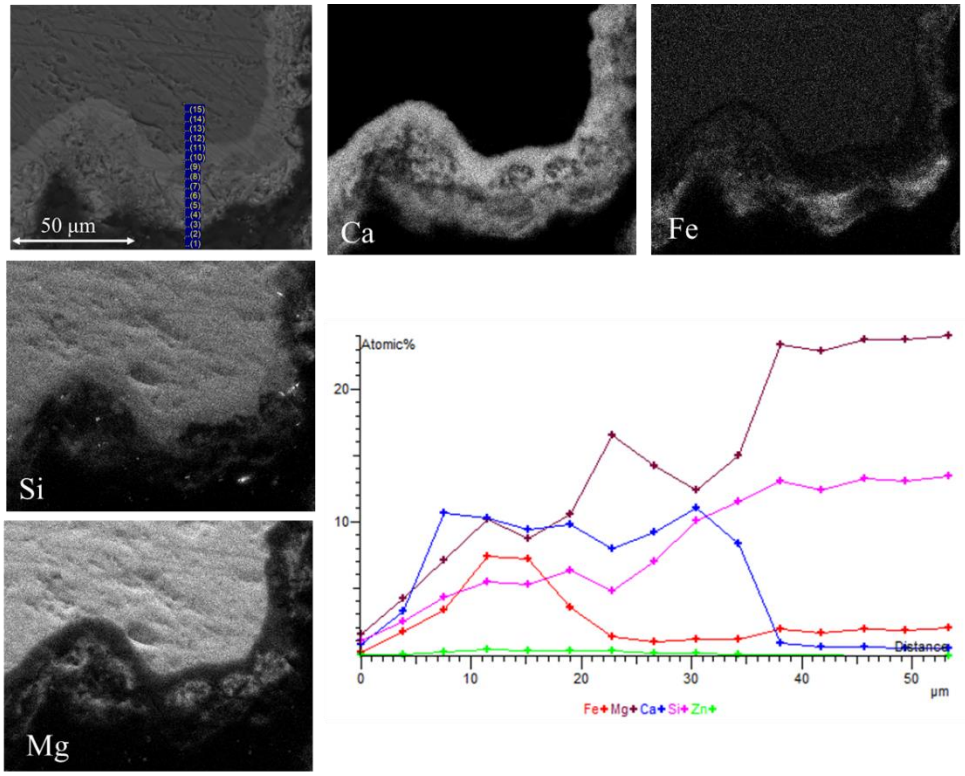

Figure 14. SEM micrograph of an olivine particle cross section obtained after 13 days of CLG with ASR. Corresponding EDX intensity maps shows the elemental distribution and the chemical composition over the ash layer acquired with line scan.

To investigate the presence of Cu and Zn in more detail, samples were investigated with XPS. As observed in Figure 14 the Zn and Cu contents are increased at the surface where the Fe-concentration is higher. During XPS measurements this was confirmed as higher Cu and Zn concentrations were observed along with Fe. XPS region spectra confirmed the presence of $CuFe_2O_4$ and $ZnFe_2O_4$. Thus, the Fe content is seemingly important as an interaction path between the bed material and Cu and Zn, not unlike the findings with ilmenite. Furthermore, investigation of the corresponding fly ash by SEM-EDX and XPS suggest formation of Cu and Zn chlorides and ferrites. Lead chlorides could also be observed. For further information regarding the fly ash, see **Paper IV**.

4.6.Phase Prediction and Characterization after OCAC and CLG

Global TEC were used in **Paper II-IV** for phase prediction using elemental analyses and operation data such as temperature and mass flows. A summary of the predicted phases by TEC, according to amount, is presented in Table 7. In **Paper IV** the global TEC predicted the main phases for the sample obtained after 13 days with CLG. Phases which were determined experimentally by XRD is presented in Table 7. Besides the components presented in the table other minor phases such as SiO_2, Fe_2O_3 and (Mg,Fe)O could also be observed.

The major crystalline phases predicted by TEC for RWW-ilmenite at 850℃ was rutile and corundum. The calculations in **Paper II** were performed to study the behavior of trace elements in presence of ilmenite which is why the oxygen carrier was determined to be in excess during TEC. The experimentally determined crystalline phases by XRD included Fe_2TiO_5 and $Fe_3Ti_3O_{10}$. However, it should be noted that the XRD spectrum for these two compounds only differ a few peaks and can be difficult to separate. Evident from Table 7 is that several compounds have been identified, but it should be noted that the diffractograms also showed peaks that were not possible to identify. Besides identified compounds presented in Table 7 for RWW-ilmenite, SiO_2 and $NaAlSiO_4$ could also be observed.

Table 7 A comparison between predicted phases by global thermodynamic equilibrium calculations and experimentally observed crystalline phases by XRD.[*]

RWW-ilmenite		MSW-ilmenite		ASR-Olivine	
Paper II		Paper III		Paper IV	
TEC	XRD	TEC	XRD	TEC	XRD
TiO_2	‡	$NaAlSi_3O_8$	xx	$Mg(Mg,Ca,Fe)SiO_4$	xxx
Fe_2O_3	‡	$CaTiO_3$	xxx	$Ca(Mg,Fe)Si_2O_6$	xxx
$CaTiO_3$	xxx	Fe_2O_3	‡	$(Fe,Mg,Zn)_3O_4$	xx
$KAlSi_3O_8$	xx	$Ca(Mg,Fe)Si_2O_6$	xx	$NaAlSiO_4$	x
$CaMgSi_2O_6$	x	TiO_2	‡	$KAlSi_3O_8$	xx
$(Fe,Mg,Zn)_3O_4$	xxx	$(Fe,Mg,Zn)_3O_4$	xxx	K_2SO_4	x
K_2SO_4	-	$CaSO_4$	x	$CaTiO_3$	x
		$NaAlSiO_4$	x		

[*] xxx, major; xx, minor; x, trace

‡ Fe_2TiO_5 was observed (Fe_2O_3 + TiO_2)

In **Paper III** a series of samples were investigated where a silica sand bed was gradually replaced with ilmenite for combustion via OCAC. Table 7 presents predicted phases by TEC for an ilmenite bed at 850℃ during OCAC with MSW, **Paper III**. The predicted phases by TEC are compared with a diffractogram for a sample obtained after 893h of OCAC with MSW. While calculations predict Fe_2O_3 and TiO_2 the crystalline phase Fe_2TiO_5 was identified by XRD. Besides the experimentally identified phases in Table 7, SiO_2, $CaMgAlSi_2O_7$ and Al_2O_3 could also be observed by XRD. It is shown in **Paper III** that the magnetic separated ash

fraction contains crystalline phases more aligned with TEC for an ilmenite bed while the rejected ash fraction is more aligned with the TEC results for a silica sand bed.

4.6.1. Parameter Variation During OCAC

Paper III investigated the influence of temperature, reduction potential, concentration of S and Cl and the choice of bed material. It was shown that mixing ilmenite with silica sand will increase the risk of slag formation. The risk is further elevated when increasing bed temperatures beyond 950°C. An increase in slag formation with temperature can be observed in Figure 15. The figure presents the phase distribution obtained by TEC across a temperature range for OCAC of MSW with a bed consisting of ilmenite and silica sand.

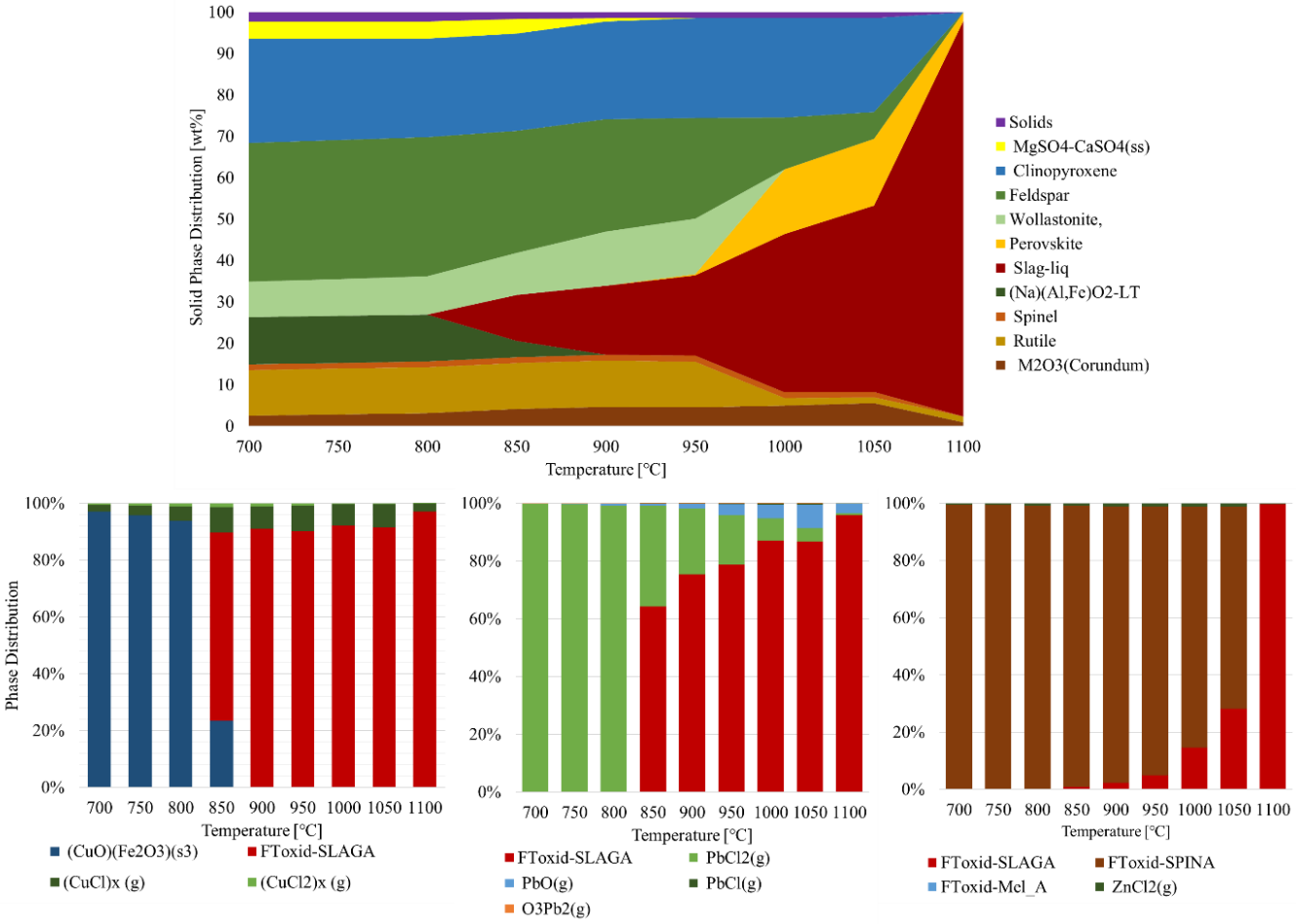

Figure 15. Global TEC of MSW between 700°C and 1100°C and 0.05 atm O_2 in the gas phase. Solid phase distribution during combustion performed with equally mixed bed with silica sand and ilmenite (top figure). Bottom figures: phase distribution of copper (left), lead (middle) and zinc (right).

The presence of alkalis can lower the melting point of the silica sand bed material. This can be observed in Figure 15 where a temperature increase shift the equilibrium from SiO_2 and feldspars $(Na,K)AlSi_3O_8$ to a slag phase (SiO_2 and $(K,Na)AlO_2$). Studying bottom ash samples reveal that some melts have formed. Figure 16 presents two surface micrographs and one cross-section micrograph of a melt. Left figure shows several ilmenite particles are connected by a melt. The middle figure shows a much larger piece of melt with particles adhered to the surface, the cross-section micrograph reveal that both sand particles (dark particles) and ilmenite particles (lighter particles) are present in this melt.

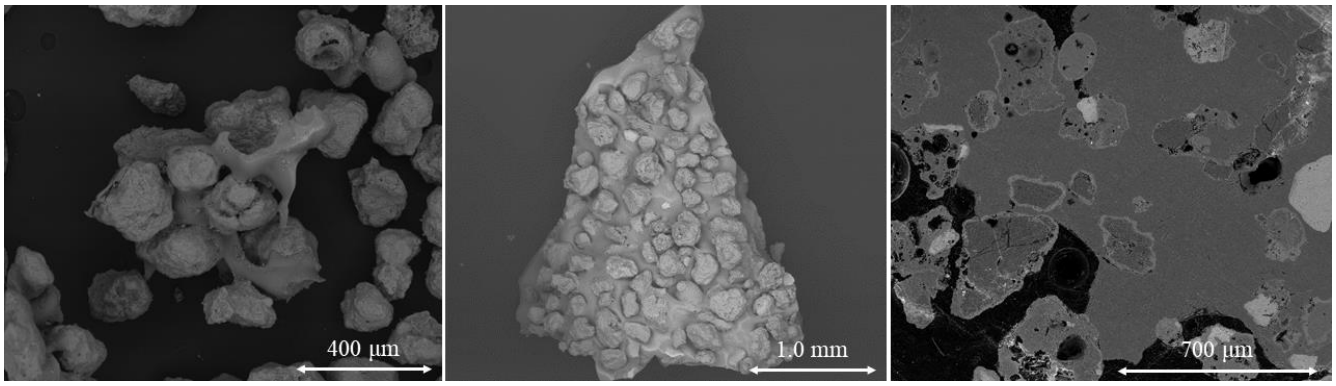

Figure 16. Top view SEM micrographs of observed melt formation with agglomeration (left figure). A piece of melt with particles attached (middle figure) along with cross section micrograph of the melt (right figure). Sample obtained after 24 days with OCAC operation with MSW at Händelö plant, bed temperature around ~930°C.

The phase distribution of Cu, Pb and Zn over a temperature range is presented in Figure 15. With increasing temperature Cu and Pb dissolve in the slag phase as Cu_2O and PbO while Zn is stable as $ZnFe_2O_4$. The results for a pure ilmenite bed show that $CuFe_2O_4$ is stable up to 950°C, Pb forms mainly $PbCl_2$ (g) up to 950°C before dissolving in the slag phase and Zn is mainly stable as $ZnFe_2O_4$ up to 1100°C. It is observed that the volatility of these elements increases according to Zn<Cu<Pb. TEC was further used to study an increase in fuel bound S and Cl. By increasing Cl, the HCl-concentration increases in the gas phase along with alkali chlorides, which slightly decreases the amount of slag phase. Other metal chlorides also form, mainly $PbCl_2$ and $(CuCl)_x$. Zn only shows a slight increase in volatility due to Cl-increase.

On the other hand, increasing the amount of S will increase SO_2 in the gas phase along with $CaSO_4$ in the solid phase. The addition of S will also result in an increase in slag phase. Since the presence of Ca and Mg silicates increase the melting point of silicate mixtures [101] more Ca associated with $CaSO_4$ will result in an increase in slag phase formation. Furthermore, addition of S will decrease the amount of alkali and metal chlorides in the gas phase which is beneficial with respect to corrosion. The major slag phase components are SiO_2 and $(K,Na)AlO_2$ and the alkali concentration in the slag phase will increase slightly. Even if the formed slag phase consists of lower concentrations of PbO and Cu_2O the increased amount of slag will result in more Pb and Cu being associated with slag. To summarize, the following has been observed during combustion utilizing an ilmenite bed:

- The operating temperature can be higher when utilizing ilmenite as an OC, compared with silica sand, before experiencing melt formation.
- An increase in temperature will aid formation of gaseous metal chlorides (especially Pb and Cu). The melt forming above 950°C will retain part of these elements in the bed. Zn is stable as a ferrite $ZnFe_2O_4$ up to 1050°C.
- Increase in the reduction potential from oxidizing to moderately reducing conditions (Between the reduction potential -8 and -4, see *Table 5*)
    - Cu undergoes the reduction $CuFe_2O_4$ → $Cu_2Fe_2O_4$ → Cu accompanied by an increase in gaseous $(CuCl)_x$
    - Pb mainly forms $PbCl_2$ with increasing amount of PbCl.
    - Zn is stable in a spinel formation mainly as $ZnFe_2O_4$ with increasing amount of $Zn(Cr,Ni)_2O_4$
  - During highly reducing conditions, above the reduction potential -2.
    - Cu mainly forms Cu_2S

- Pb forms PbS(g) with increasing amount of Pb (g)
- Zinc is distributed between melilite ($Ca_2ZnSi_2O_7$), spinel ($Zn(Cr,Ni)_2O_4$) and gaseous Zn (g). With increasing reduction potential Zn (g) increases along with a slag phase (ZnS).

- Increased fuel Cl-concentrations will favor formation of gaseous $(CuCl)_x$ and $PbCl_2$ while increased S-concentrations could be beneficial for dissolving part of PbO in the melt. The Zn-distribution was only slightly affected by changes in Cl.

5. Discussion

In this thesis the interaction between trace elements and different oxygen carrier material has been studied. Before the start of this work there were no investigations conducted regarding the interaction between trace elements, Cu, Zn and Pb and oxygen carriers during combustion and gasification. To study the interactions of these metals in the highly complex environment of combustion and gasification, a combined thermodynamic and experimental approach was used. Samples have been obtained from a range of sources, from laboratory to industrial scale facilities. With respect to the latter, three semi-commercial and commercial units used here operated for many weeks using oxygen carriers and waste fuels. Thus, highly relevant samples have been retrieved, where the residence times of particles are expected to be long enough for significant trace element interaction and for thermodynamic stable phases to form.

The advantage with the theoretical approach using thermodynamic equilibrium calculations is the possibility to investigate a wide range of parameters, such as temperature and reduction potential. It accounts for all known and verified phases and interactions in the system and gives an overview of the main phase formation and trace element distribution. However, the reactions in the boiler will also depend on other factors such as kinetics and physical phenomena which are not accounted for during TEC. For example, the particle surfaces will change due to interaction with ash components, melting or migration of elements, for example migration of Fe in the bed material. This will change the chemical components that are available to the surrounding gas phase and will affect equilibrium. To account for this, global calculations have been complemented with local TEC which are performed on specific particles to investigate the surface composition. This enables a direct comparison between the chemical states observed in XPS-measurements and thermodynamic predictions. The accuracy of these calculations largely depends on the defined parameters and databases. The agreement between experiments and thermodynamic predictions is shown to be largely in line. However, there are some subsystems which require further studies. Some database improvement has been made in this thesis. In **Paper II** it was observed that data is scarce regarding lead silicates and copper aluminates, and some of these compounds were added to the HSCA-database in **Paper III**, see Appendix. Despite this, more work is needed to further identify the limitations and improve the databases by optimization and addition of compounds.

Based on this combinatorial approach the fate of trace elements has been studied and it has been shown that the chemistry can vary compared with regular fluidized bed combustion. The mechanisms and pathways observed in this thesis will be summarized below and the implication on chemical looping processes will be discussed.

5.1. Main Interaction Paths

It has been shown that the silica-alkali-Cl relation is important for slag phase formation, but also the partitioning of heavy metals. A summary of the main pathways for Zn, Cu and Pb based on thermodynamic calculations and experimental findings is illustrated for CLG of ASR in Figure 17 (left) and OCAC of MSW (right).

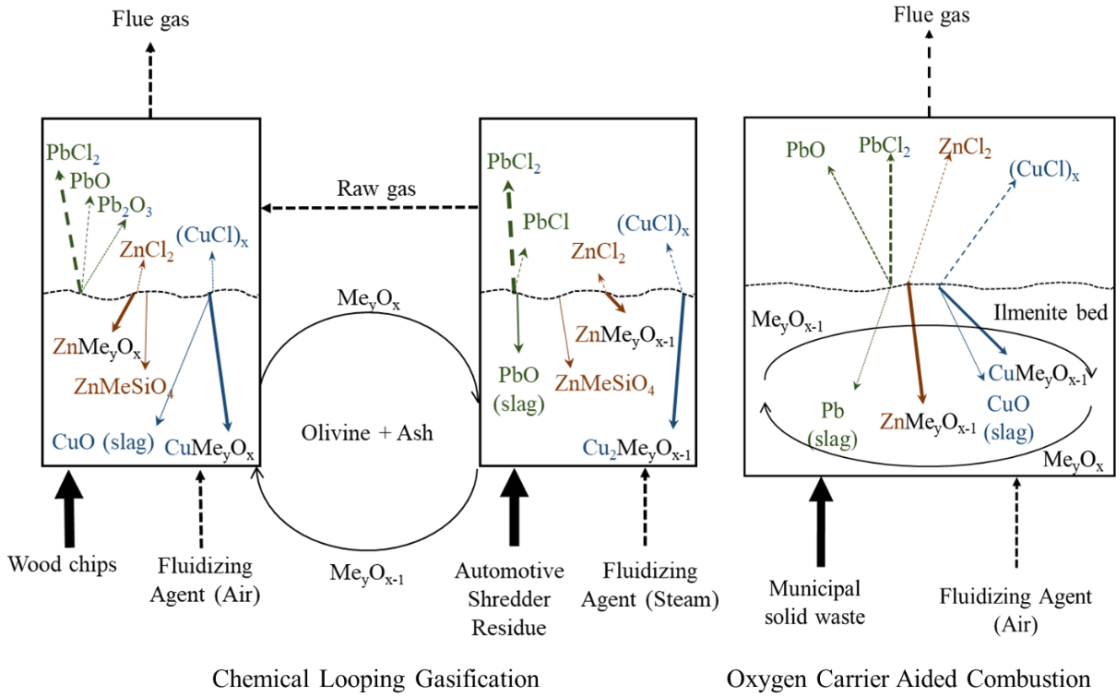

*Figure 17. A summary of the main interaction paths for Zn, Cu and Pb in CLG of ASR (left) and OCAC of MSW (right). Based on TEC and experimental findings from **Paper II-IV**. Dashed arrows represent gas flows and solid arrows represent phases in the bed. Main compound formation is indicated by thicker arrows.*

During CLG, the reduction potential is higher in the gasifier compared to the boiler. This has implication for trace element oxidation state, for instance, formation of Cu^{+} in the gasifier and Cu^{2+} in the boiler. Summarizing, Pb is found to mainly enter the gas phase as $PbCl_2$ while both Zn and Cu are expected to mainly form ferrites in the gasifier. As this semi-industrial setup is used for research purposes the raw gas is not utilized, instead it is fed back to the boiler. But in a commercial process, this raw gas stream would be separated from the boiler, and the major amount of Pb can be expected to be recovered in this stream. In the boiler Cu and Zn remain mainly in the form of ferrites.

In contrast to CLG, OCAC is realized using only one bed and the reduction potential is not altered as heavily as during CLG or CLC, in comparison to normal fluidized bed combustion. TEC in **Paper III** illustrated that the gas-solid equilibrium can be altered by changing bed material, temperature, reduction potential and by chemical additions. Looking back at the classification of heavy metals during combustion, Figure 3, it is clear that the presence of OCs has changed the volatilization behavior of the TEs, and mainly the element Zn is affected. Zn can be expected to be less volatile, and hence moved from class III to class I in the figure, in principle due to enrichment as zinc ferrite in the bottom ash. Further, Cu is moved from in-between class III and II to between class I and II since it is not concentrated in the fly ash but rather fairly distributed between the BA and FA. Although some interaction between OC and Pb was determined, the extent of the reaction is not sufficient to change the classification from class III and Pb is expected to mainly be concentrated in the FA.

These shifts in metal concentration from FAs to BAs could have implications for boiler performance and corrosion in addition to the subsequent treatment of the ashes. For example, corrosion during combustion of recycled waste wood has been shown to be caused by heavy

metals or by a combination of heavy metals and alkali chlorides [59, 102, 103]. Thus, lower metal concentrations in the FA could be beneficial with respect to corrosion but also toxicity. Treatment of ashes could be of interest to make them less toxic or perhaps also for metal recovery. The amount of produced fly and bottom ashes are fairly equal and neglecting the bottom ash could result in loss of valuable metals. Pb will likely continue to be concentrated in the FA when utilizing oxygen carriers and possible extraction procedures should therefore concentrate on this ash fraction when it comes to Pb. On the other hand, formation of Cu and Zn ferrites will likely cause enrichment of these metals in the BA. The identified Cu and Zn ferrites could also have oxygen carrying capabilities. For example, both Cu ferrites [90, 104] and Zn ferrites [105] have previously been studied as oxygen carriers. This opens for the possibility to increase oxygen carrying capacity of the bed as the residence time increases, something which would be highly beneficial. However, the influence on the oxygen carrying capability due to interaction with ash components, such as Cu and Zn, has not been studied and thus in need of further research. Furthermore, the enrichment of Cu and Zn in the BA suggest that more attention will be needed on the extraction possibilities from the bottom ashes and further studies are required to investigate possible extraction methods.

5.2.Implications for Chemical Looping Processes

The primary technology investigated here is OCAC, which has many advantages with respect to normal combustion. It can also be seen as a first step towards deployment of carbon capture via CLC. It can be expected that the first commercial utilization of CLC would also use ilmenite, as it is currently the bench-mark oxygen carrier also in CLC pilots [34]. The results obtained for different reduction potentials can provide insights on the phase formation in a CLC fuel reactor. Since there is no oxygen added in form of air, the reduction potential will be higher in the FR, around $\log_{10}[pCO/pCO_2] = -2$, based on settings in **Paper I**. A summary of predicted phases during CLC is presented in Figure 18.

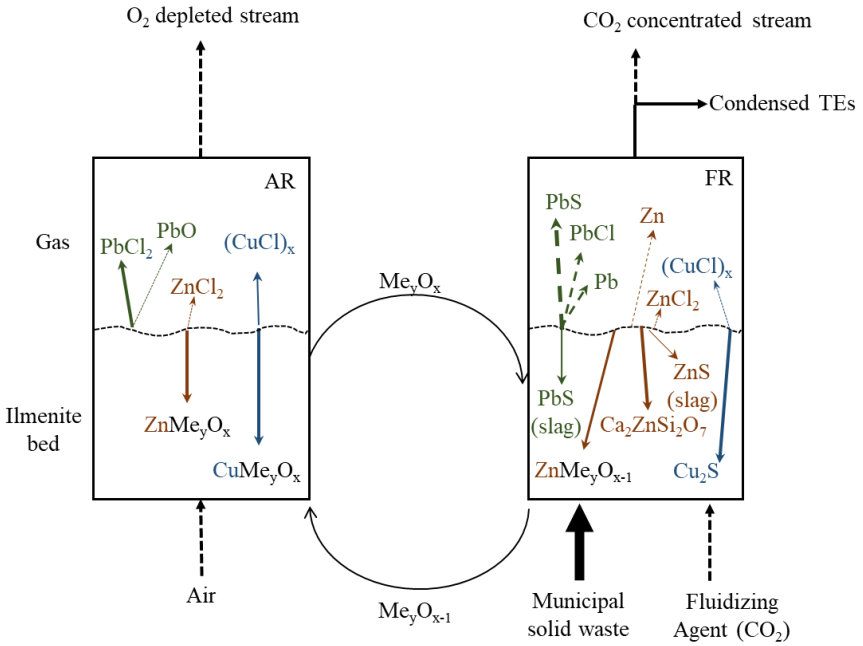

Figure 18. Predicted phase distribution of Zn, Cu and Pb in CLC of MSW. Based on calculations for 850°C, 1 atm and a reduction potential of -2 (FR) and -8 (AR). Dashed arrows represent TE gas flows and solid arrows represent TE phases in the bed. Phase distribution is indicated by the thickness of the arrows.

It can be observed in Figure 18 that Pb will be released to the gas phase in the FR mainly as PbS (g), a compound not as corrosive as chlorides. Zn and Cu are concentrated in the bottom ash as $Ca_2ZnSi_2O_7$, $ZnMe_yO_{x-1}$ and Cu_2S. Concentrating the corrosive products (alkali and metal chlorides) in the FR will avoid corrosion attacks on the heat transfer surfaces in the AR, where most of the heat is recovered [106]. This could also be beneficial for recovery of these metals, but this field of research requires more in-depth studies. The solid compounds are transferred from the FR to the AR, where oxidation of the OC occurs. The circulating solids will transport heat from the AR to the FR. This results in a slight temperature difference where the AR is generally 50°C higher [107]. It is important to note that an increase in temperature could affect the predicted phase distribution, especiallt formation of melts, but also the metal volatility. In Figure 18 it can also be observed that mainly Cu and Zn ferrites are stable in the AR and no or minor release to the gas phase is expected. Since most of the Pb is released in the FR this leaves only a small amount of PbO which could possibly be released in the AR. The elemental composition presented in Table 6 show that a significantly higher metal concentration is obtained by magnetic separation, especially regarding the TEs Zn and Cr. Using a magnetic separator between the FR and AR to separate the oxygen carriers from the inert ash components could improve the oxygen carrier efficiency of the bed. Simultaneously, by removing inert ash components such as silicates from the bed could decrease the risk of melt formation. The summary presented in Figure 18 is based on the experimental and theoretical results obtained from OCAC with MSW at 850°C. Thus, it is proposed that future studies utilize the global thermodynamic approach presented in this thesis on a CLC system to further investigate TE phase distribution in the AR and FR. Preferably in combination with ash samples subjected to CLC-conditions.

6. Conclusion

The aim of this thesis has been to investigate the phase distribution of Zn, Cu and Pb during thermochemical conversion of waste fuels. This is the first comprehensive study in this area, and a combination of equilibrium calculations and particle characterization of oxygen carriers from different units was used to gain better understanding. These trace elements can have implications with respect to boiler performance and ash characteristics. It is shown that the boiler chemistry is affected by the presence of oxygen carriers. More specifically, it is shown that utilizing ilmenite during OCAC of waste provide certain benefits compared with fluidized bed combustion with silica sand. With an ilmenite bed it is possible to reach higher temperatures with lower fraction of melts. Further, utilizing ilmenite as an oxygen carrier affects the phase distribution of trace elements. Zn is shown to be influenced the most by the presence of ilmenite and the enrichment in the bottom ashes can be attributed to the incorporation of Zn in the formed ash layer. To some extent Cu is also affected, due to enrichment in the particle core. Less Cu and Zn in downstream parts of the boiler could reduce corrosion but also result in a more benign fly ash fraction. Furthermore, both Zn and Cu were identified in the form of ferrites which could act as oxygen carriers themselves. Pb is the element least affected, only some Pb chlorides and titanates could be observed on the particle surface.

Using olivine and the metal rich fuel ashes as oxygen carrier in chemical looping gasification showed that Cu and Zn were mainly concentrated at the particle surface while only minor amounts of Pb were observed on the surface indicating that most is released to the gas phase. The surface enrichment of Cu and Zn is mainly due to the high Fe content. Thus, Fe is seemingly important as an interaction path between the bed material and Cu and Zn, and in the same way as with OCAC this could have certain advantages with respect to corrosion and ash characteristics.

Thermodynamic equilibrium calculations were used to predict the phase formation and to study the effect of parameter variation. It is shown that the calculations performed are not only valuable as comparison with phase characterization but also for providing information regarding the boiler chemistry and parameter study, not only for combustion but also for gasification. Although the calculations in this thesis were performed using waste fuels the choice of fuel and bed material is not limited and the compiled database can be utilized for other purposes.

Nomenclature

AFR	Air to Fuel Ratio
AR	Air Reactor
BA	Bottom Ash
BECCS	Bio-Energy with Carbon Capture and Storage
CCA	Copper Chromated Arsenic
CFB	Circulating Fluidized Bed
CLC	Chemical Looping Combustion
CLG	Chemical Looping Gasification
DFB	Dual Fluidized Bed
ELV	End-of-Life Vehicles
FA	Fly Ash
FBC	Fluidized Bed Combustion
FR	Fuel Reactor
GHG	Greenhouse Gas
MSW	Municipal Solid Waste
OCAC	Oxygen Carrier Aided Combustion
PVC	Polyvinyl Chloride
SEM	Scanning Electron Microscopy
TE	Trace Elements
TEC	Thermodynamic Equilibrium Calculation
WtE	Waste to Energy
c_p	Heat capacity
G	Gibbs energy
G_m^{Φ}	Molar Gibbs energy of phase Φ
H_f°	Standard enthalpy of formation (1 bar and 298.15 K)
ΔH_t	Enthalpy change during phase transition
L_{ij}	Interaction parameter
$L(n, M)$	Lagrangian function
M_j	Lagrange multiplier
S_f°	Standard entropy of formation (1 bar and 298.15 K)
n_i^{Φ}	Molar quantity of phase constituent i in phase Φ
$a_{i,j}$	Stoichiometric coefficient
b_j	Molar quantity of system component j
μ_i	Chemical potential of specie i

References

[1] IPCC. Climate change 2014: Mitigation of climate change. Contribution of working group iii to the fifth assessment report of the intergovernmental panel on climate change. In: Edenhofer O, Pichs-Madruga R, Sokona Y, Farahani E, Kadner S, Seyboth K, et al., editors. Cambridge, United Kingdom and New York, USA2014.
[2] IPCC. Summary for policymakers. In: Global warming of 1.5°c. An ipcc special report on the impacts of global warming of 1.5°c above pre-industrial levels and related global greenhouse gas emission pathways, in the context of strengthening the global response to the threat of climate change, sustainable development, and efforts to eradicate poverty. In: V. Masson-Delmotte, P. Zhai, H. O. Pörtner, D. Roberts, J. Skea, P. R. Shukla, et al., editors. Geneva, Switzerland.2018. p. 32 pp.
[3] Fuss S, Canadell JG, Peters GP, Tavoni M, Andrew RM, Ciais P, Jackson RB, Jones CD, Kraxner F, Nakicenovic N, Le Quéré C, Raupach MR, Sharifi A, Smith P, Yamagata Y. Betting on negative emissions. Nature Climate Change. 2014;4:850.
[4] Gasser T, Guivarch C, Tachiiri K, Jones CD, Ciais P. Negative emissions physically needed to keep global warming below 2°c. Nature Communications. 2015;6.
[5] Azar C, Lindgren K, Obersteiner M, Riahi K, van Vuuren DP, den Elzen KMGJ, Möllersten K, Larson ED. The feasibility of low co2 concentration targets and the role of bio-energy with carbon capture and storage (beccs). Climatic Change. 2010;100:195-202.
[6] Barker T., I. Bashmakov, L. Bernstein, J. E. Bogner, P. R. Bosch, R. Dave, O. R. Davidson, B. S. Fisher, S. Gupta, K.Halsnæs, G.J. Heij, S. Kahn Ribeiro, S. Kobayashi, M. D. Levine, D. L. Martino, O. Masera, B. Metz, L. A. Meyer, G.-J. Nabuurs, A. Najam, N. Nakicenovic, H. -H. Rogner, J. Roy, J. Sathaye, R. Schock, P. Shukla, R. E. H. Sims, P. Smith, D. A. Tirpak, D. Urge-Vorsatz, Zhou D. Technical summary. In: Climate change 2007: Mitigation. Contribution of working group iii to the fourth assessment report of the intergovernmental panel on climate change In: B. Metz, O. R. Davidson, P. R. Bosch, R. Dave, Meyer LA, editors. Cambridge University Press, Cambridge, United Kingdom and New York, NY, USA.2007.
[7] IPCC. Climate change 2013: The physical science basis. Contribution of working group i to the fifth assessment report of the intergovern-mental panel on climate change In: Stocker TF, D. Qin, G.-K. Plattner, M. Tignor, S.K. Allen, J. Boschung, et al., editors. Cambridge University Press, Cambridge, United Kingdom and New York, NY, USA.2013. p. 1535.
[8] Kormi T, Bel Hadj Ali N, Abichou T, Green R. Estimation of landfill methane emissions using stochastic search methods. Atmospheric Pollution Research. 2017;8:597-605.
[9] Sharma Kapil D, Jain S. Municipal solid waste generation, composition, and management: The global scenario. Social Responsibility Journal. 2020;16:917-48.
[10] Eurostat. Municipal waste by waste management operations. Dataset: ENV_WASMUN: European Commission.
[11] EuropeanCommission. Communication from the commission to the european parliament, the council, the european economic and social committee and the committee of the region - the role of waste-to-energy in the circular economy. Brussels2017.
[12] Khandelwal H, Dhar H, Thalla AK, Kumar S. Application of life cycle assessment in municipal solid waste management: A worldwide critical review. Journal of Cleaner Production. 2019;209:630-54.
[13] Lam CHK, Ip AWM, Barford JP, McKay G. Use of incineration msw ash: A review. Sustainability. 2010;2.
[14] Svensk avfallshantering 2019. Avfall Sverige 2019.

[15] Johansson I, Sahlin E, von Bahr B, Björkmalm J, Todorovic olsson J. Kritiska metaller i svenska avfallsaskorthe content of critical elements in residues from swedish waste-to -energy plants. Waste Refinery. 2013.
[16] Edo M, Björn E, Persson P-E, Jansson S. Assessment of chemical and material contamination in waste wood fuels – a case study ranging over nine years. Waste Management. 2016;49:311-9.
[17] Karlfeldt Fedje K, Andersson S. Zinc recovery from waste-to-energy fly ash – a pilot test study. Waste Management. 2020;118:90-8.
[18] Schlumberger S, Schuster M, Ringmann S, Koralewska R. Recovery of high purity zinc from filter ash produced during the thermal treatment of waste and inerting of residual materials. Waste management & research : the journal of the International Solid Wastes and Public Cleansing Association, ISWA. 2007;25:547-55.
[19] Tang J, Steenari B-M. Leaching optimization of municipal solid waste incineration ash for resource recovery: A case study of cu, zn, pb and cd. Waste Management. 2016;48:315-22.
[20] Nagib S, Inoue K. Recovery of lead and zinc from fly ash generated from municipal incineration plants by means of acid and/or alkaline leaching. Hydrometallurgy. 2000;56:269-92.
[21] Thunman H, Lind F, Breitholtz C, Berguerand N, Seemann M. Using an oxygen-carrier as bed material for combustion of biomass in a 12-mwth circulating fluidized-bed boiler. Fuel. 2013;113:300-9.
[22] Zevenhoven R, Kilpinen P. Control of pollutants in flue gases and fuel gases. Finland2001.
[23] Ma W, Wenga T, Frandsen FJ, Yan B, Chen G. The fate of chlorine during msw incineration: Vaporization, transformation, deposition, corrosion and remedies. Progress in Energy and Combustion Science. 2020;76:100789.
[24] Pedersen AJ, Frandsen FJ, Riber C, Astrup T, Thomsen SN, Lundtorp K, Mortensen LF. A full-scale study on the partitioning of trace elements in municipal solid waste incineration—effects of firing different waste types. Energy & Fuels. 2009;23:3475-89.
[25] Strömberg B. Miljö- och förbränningsteknik - bränslehandboken. Värmeforsk, Värmeteknisk Forskning och Arbete: Värmeforsk; 2005.
[26] Humar M, Jermer J, Peek R. Regulations in the european union with emphasis on germany, sweden and slovenia. 2006. p. 37-57.
[27] Cossu R, Lai T. Automotive shredder residue (asr) management: An overview. Waste Management. 2015;45:143-51.
[28] Gonzalez-Fernandez O, Hidalgo M, Margui E, Carvalho ML, Queralt I. Heavy metals' content of automotive shredder residues (asr): Evaluation of environmental risk. Environmental Pollution. 2008;153:476-82.
[29] Zevenhoven R, Saeed L. Automotive shredder residue (asr) and compact disc (cd) waste options for recovery of materials and energy. Helsinki University of Technology, Espoo (Finland). 2003.
[30] Krook J, Mårtensson A, Eklund M. Metal contamination in recovered waste wood used as energy source in sweden. Resources, Conservation and Recycling. 2004;41:1-14.
[31] Determination of the fossil carbon content in combustible municipal solid waste in sweden. Avfall Sverige Utveckling Report U2012:02; 2012.
[32] Pissot S, Berdugo Vilches T, Maric J, Cañete Vela I, Thunman H, Seemann M. Thermochemical recycling of automotive shredder residue by chemical-looping gasification using the generated ash as oxygen carrier. Energy & Fuels. 2019;33:11552-66.
[33] Larsson A, Seemann M, Neves D, Thunman H. Evaluation of performance of industrial-scale dual fluidized bed gasifiers using the chalmers 2–4-mwth gasifier. Energy & Fuels. 2013;27:6665-80.

[34] Mattisson T, Keller M, Linderholm C, Moldenhauer P, Rydén M, Leion H, Lyngfelt A. Chemical-looping technologies using circulating fluidized bed systems: Status of development. Fuel Processing Technology. 2018;172:1-12.
[35] Moldenhauer P, Gyllén A, Thunman H, Lind F. A scale-up project for operating a 115 mwth biomass-fired cfb boiler with oxygen carriers as bed material. 2018.
[36] Lind F, Corcoran A, Andersson B, Thunman H. 12,000 hours of operation with oxygen-carriers in industrially relevant scale (75,000 kwth). VGB PowerTech. 2017.
[37] This is improbed™ - improbed. Malmö, Sweden.
[38] Dong C, Jiang J, Yang Y, Zhang J, Shan L. Research on the reactivity of oxygen carrier fe2o3 for chemical looping combustion (clc). Asia-Pacific Power and Energy Engineering Conference, APPEEC2010.
[39] Jerndal E, Mattisson T, Lyngfelt A. Thermal analysis of chemical-looping combustion. Chemical Engineering Research and Design. 2006;84:795-806.
[40] Abad A, Adánez J, García-Labiano F, de Diego LF, Gayán P, Celaya J. Mapping of the range of operational conditions for cu-, fe-, and ni-based oxygen carriers in chemical-looping combustion. Chemical Engineering Science. 2007;62:533-49.
[41] Mendiara T, Abad A, de Diego LF, García-Labiano F, Gayán P, Adánez J. Biomass combustion in a clc system using an iron ore as an oxygen carrier. International Journal of Greenhouse Gas Control. 2013;19:322-30.
[42] Linderholm C, Schmitz M. Chemical-looping combustion of solid fuels in a 100 kw dual circulating fluidized bed system using iron ore as oxygen carrier. Journal of Environmental Chemical Engineering. 2016;4:1029-39.
[43] Knutsson P, Linderholm C. Characterization of ilmenite used as oxygen carrier in a 100 kw chemical-looping combustor for solid fuels. Applied Energy. 2015;157:368-73.
[44] Cuadrat A, Abad A, García-Labiano F, Gayán P, de Diego LF, Adánez J. The use of ilmenite as oxygen-carrier in a 500wth chemical-looping coal combustion unit. International Journal of Greenhouse Gas Control. 2011;5:1630-42.
[45] Moldenhauer P, Rydén M, Mattisson T, Younes M, Lyngfelt A. The use of ilmenite as oxygen carrier with kerosene in a 300 w clc laboratory reactor with continuous circulation. Applied Energy. 2014;113:1846-54.
[46] Liu F, Zhang Y, Chen L, Qian D, Neathery JK, Kozo S, Liu K. Investigation of a canadian ilmenite as an oxygen carrier for chemical looping combustion. Energy and Fuels. 2013;27:5987-95.
[47] Bao J, Li Z, Cai N. Interaction between iron-based oxygen carrier and four coal ashes during chemical looping combustion. Applied Energy. 2014;115:549-58.
[48] Niu Y, Tan H, Hui S. Ash-related issues during biomass combustion: Alkali-induced slagging, silicate melt-induced slagging (ash fusion), agglomeration, corrosion, ash utilization, and related countermeasures. Progress in Energy and Combustion Science. 2016;52:1-61.
[49] Gatternig B, Karl J. Investigations on the mechanisms of ash-induced agglomeration in fluidized-bed combustion of biomass. Energy and Fuels. 2015;29:931-41.
[50] Gu H, Shen L, Zhong Z, Zhou Y, Liu W, Niu X, Ge H, Jiang S, Wang L. Interaction between biomass ash and iron ore oxygen carrier during chemical looping combustion. Chemical Engineering Journal. 2015;277:70-8.
[51] Hanning M, Gyllén A, Lind F, Rydén M. Biomass ash interactions with a manganese ore used as oxygen-carrying bed material in a 12 mwth cfb boiler. Biomass and Bioenergy. 2018;119:179-90.
[52] Vigoureux M, Knutsson P, Lind F. Sulfur uptake during oxygen-carrier-aided combustion with ilmenite. Energy & Fuels. 2020;34:7735-42.

[53] Corcoran A, Marinkovic J, Lind F, Thunman H, Knutsson P, Seemann M. Ash properties of ilmenite used as bed material for combustion of biomass in a circulating fluidized bed boiler. Energy and Fuels. 2014;28:7672-9.
[54] Corcoran A, Knutsson P, Lind F, Thunman H. Mechanism for migration and layer growth of biomass ash on ilmenite used for oxygen carrier aided combustion. Energy and Fuels. 2018;32:8845-56.
[55] Gyllén A, Knutsson P, Lind F, Thunman H. Magnetic separation of ilmenite used as oxygen carrier during combustion of biomass and the effect of ash layer buildup on its activity and mechanical strength. Fuel. 2020;269:117470.
[56] Hildor F, Zevenhoven M, Brink A, Hupa L, Leion H. Understanding the interaction of potassium salts with an ilmenite oxygen carrier under dry and wet conditions. ACS Omega. 2020;5:22966-77.
[57] Backman R, Hupa M, Hiltunen M, Peltola K. Interaction of the behavior of lead and zinc with alkalis in fluidized bed combustion or gasification of waste derived fuels. 18th International Conference on Fluidized Bed Combustion. 2005.
[58] Khan AA, de Jong W, Jansens PJ, H. S. Biomass combustion in fluidized bed boilers: Potential problems and remedies. Fuel Processing Technology. 2009;90:21-50.
[59] Spiegel M. 1.14 - corrosion in molten salts. In: Cottis B, Graham M, Lindsay R, Lyon S, Richardson T, Scantlebury D, et al., editors. Shreir's corrosion. Oxford: Elsevier; 2010. p. 316-30.
[60] Hupa M. Ash-related issues in fluidized-bed combustion of biomasses: Recent research highlights. Energy and Fuels. 2012;26:4-14.
[61] Kinnunen H, Hedman M, Lindberg D, Enestam S, Yrjas P. Corrosion in recycled wood combustion—reasons, consequences, and solutions. Energy & Fuels. 2019;33:5859-66.
[62] Camerani M, Somogyi A, Drakopoulos M, Steenari B. Synchrotron radiation induced μ–x-ray fluorescence spectroscopy on municipal solid waste fly ashes. Spectrochimica Acta Part B. 2001;56:1355-65.
[63] Camerani Pinzani M. Cadmium distribution and speciation by synchrotron radiation induced x-ray microprobe technologies. Gothenburg: Chalmers University of Technology; 2003.
[64] Golding A, Bigelow C, Veneman L. Concentrations of metals in ash from municipal solid waste combustors. Chemosphere. 1992;24:271-80.
[65] Stinespring CD, Stewart GW. Surface enrichment of aluminosilicate minerals and coal combustion ash particles. Atmospheric Environment (1967). 1981;15:307-13.
[66] Camerani MC, Somogyi A, Vekemans B, Ansell S, Simionovici AS, Steenari B-M, Panas I. Determination of the cd-bearing phases in municipal solid waste and biomass single fly ash particles using sr-μxrf spectroscopy. Analytical Chemistry. 2007;79:6496-506.
[67] Clarke LB, Sloss LL. Trace elements - emissions from coal combustion and gasification. United Kingdom1992.
[68] Jiao F, Zhang L, Song W, Meng Y, Yamada N, Sato A, Y N. Effect of inorganic particulates on the condensation behavior of lead and zinc vapors. Proceedings of the combustion institute. 2013;34:2821-9.
[69] Leion H, Mattisson T, Lyngfelt A. Use of ores and industrial products as oxygen carriers in chemical-looping combustion. Energy and Fuels. 2009;23:2307-15.
[70] Staničić I, Andersson V, Hanning M, Mattisson T, Backman R, Leion H. Combined manganese oxides as oxygen carriers for biomass combustion — ash interactions. Chemical Engineering Research and Design. 2019;149:104-20.
[71] Staničić I, Hanning M, Deniz R, Mattisson T, Backman R, Leion H. Interaction of oxygen carriers with common biomass ash components. Fuel Processing Technology. 2020;200:106313.

[72] Moulder JM, Stickle WF, Sobol PE, Bomben Kd. Handbook of x-ray photoelectron spectroscopy - a reference book of standard spectra for identification and interpretation of xps data. 6509 Flying Cloud Drive Eden Prairie, Minnesota 55344 United Stales of America: Perkin-Elmer Corporation - Physical Electronics Division; 1992.
[73] Naumkin VA, Kraut-Vass A, Gaarenstroom SW, Powell CJ. Nist x-ray photoelectron spectroscopy database - nist standard reference database 20, version 4. 6 June 2000 ed. Gaithersburg MD, 20899: National Institute of Standards and Technology; 2012.
[74] Pelton AD. Phase diagrams and thermodynamic modeling of solutions2019.
[75] Weber CF. Convergence of the equilibrium code solgasmix. Journal of Computational Physics. 1998;145:655-70.
[76] Bale CW, Bélisle E, Chartrand P, Decterov SA, Eriksson G, Gheribi AE, Hack K, Jung IH, Kang YB, Melançon J, A. D. Pelton AD, Petersen S, Robelin C, Sangster J, Spencer P, Van Ende M-A. Factsage thermochemical software and databases - 2010 - 2016. Calphad. 2016;54:35-53.
[77] Stølen S, Grande T. Thermodynamic foundations. Chemical thermodynamics of materials2003. p. 1-27.
[78] Eriksson G. Thermodynamic studies of high temperature equilibria. Chemica Scripta. 1975;8:100-3.
[79] Smith WR, Missen RW. Chemical reaction equilibrium analysis: Wiley; 1982.
[80] Pelton AD. 15 - multiple-sublattice random-mixing (bragg-williams—bw) models. In: Pelton AD, editor. Phase diagrams and thermodynamic modeling of solutions. Amsterdam: Elsevier; 2019. p. 229-52.
[81] Chartrand P, Pelton AD. The modified quasi-chemical model: Part iii. Two sublattices. Metallurgical and Materials Transactions A. 2001;32:1397-407.
[82] Eriksson G, Königsberger E. Factsage and chemapp: Two tools for the prediction of multiphase chemical equilibria in solutions. Pure and Applied Chemistry. 2008;80:1293-302.
[83] Malcolm W. Chase, Jr. Nist-janaf thermochemical tables: Fourth edition. Washington, DC : American Chemical Society ; New York : American Institute of Physics for the National Institute of Standards and Technology, 1998.; 1998.
[84] Belov GV, Dyachkov SA, Levashov PR, Lomonosov IV, Minakov DV, Morozov IV, Sineva MA, Smirnov VN. The ivtanthermo-online database for thermodynamic properties of individual substances with web interface. Journal of Physics: Conference Series. 2018;946:012120.
[85] Dinsdale A. Sgte data for pure elements. Calphad. 1991;15:317-425.
[86] Davies RH, Dinsdale AT, Gisby JA, Robinson JAJ, Martin SM. Mtdata - thermodynamic and phase equilibrium software from the national physical laboratory. Calphad. 2002;26:229-71.
[87] Andersson JO, Helander T, Höglund L, Shi PF, Sundman B. Thermo-calc and dictra computational tools for materials science. Calphad. 2002;26:273-312.
[88] Roine. A. Hsc chemistry® [software], outotec, pori 2018.
[89] Frandsen FJ, Dam-Johansen K, Rasmussen P. Trace elements from combustion and gasification of coal—an equilibrium approach. Progress in Energy and Combustion Science. 1994;20:115-38.
[90] Darwish E, Yılmaz D, Leion H. Experimental and thermodynamic study on the interaction of copper oxygen carriers and oxide compounds commonly present in ashes. Energy & Fuels. 2019;33:2502-15.
[91] Becidan M, Sørum L, Lindberg D. Impact of municipal solid waste (msw) quality on the behavior of alkali metals and trace elements during combustion: A thermodynamic equilibrium analysis. Energy & Fuels. 2010;24:3446-55.

[92] Konttinen J, Backman R, Hupa M, Moilanen A, Kurkela E. Trace element behavior in the fluidized bed gasification of solid recovered fuels – a thermodynamic study. Fuel. 2013;106:621-31.
[93] Frandsen F, Dam-Johansen K, Rasmussen P. Gfedbase — a pure substance trace element thermochemical database. Calphad. 1996;20:175-229.
[94] Lundholm K, Nordin A, Backman R. Trace element speciation in combustion processes—review and compilations of thermodynamic data. Fuel Processing Technology. 2007;88:1061-70.
[95] Talonen T. Chemical equilibria of heavy metals in waste incineration: Comparison of thermodynamic databases [Licentiate]: Åbo Akademi University; 2008.
[96] Lindberg D, Backman R, Chartrand P, Hupa M. Towards a comprehensive thermodynamic database for ash-forming elements in biomass and waste combustion — current situation and future developments. Fuel Processing Technology. 2011;105:129-41.
[97] Kramb J, Konttinen J, Backman R, Salo K, Roberts M. Elimination of arsenic-containing emissions from gasification of chromated copper arsenate wood. Fuel. 2016;181:319-24.
[98] Enestam S, Backman R, Mäkelä K, Hupa M. Evaluation of the condensation behavior of lead and zinc in bfb combustion of recovered waste wood. Fuel Processing Technology. 2013;105:161-9.
[99] Lancee RJ, Dugulan AI, Thüne PC, Veringa HJ, Niemantsverdriet JW, Fredriksson HOA. Chemical looping capabilities of olivine, used as a catalyst in indirect biomass gasification. Applied Catalysis B: Environmental. 2014;145:216-22.
[100] Kirnbauer F, Hofbauer H. The mechanism of bed material coating in dual fluidized bed biomass steam gasification plants and its impact on plant optimization. Powder Technology. 2013;245:94-104.
[101] Billen P, Van Caneghem J, Vandecasteele C. Predicting melt formation and agglomeration in fluidized bed combustors by equilibrium calculations. Waste and Biomass Valorization. 2014;5:879-92.
[102] Bankiewicz D, Enestam S, Yrjas P, Hupa M. Experimental studies of zn and pb induced high temperature corrosion of two commercial boiler steels. Fuel Processing Technology. 2013;105:89-97.
[103] Backman R, Khalil RA, Todorovic D, Skreiberg Ø, Becidan M, Goile F, Skreiberg A, Sørum L. The effect of peat ash addition to demolition wood on the formation of alkali, lead and zinc compounds at staged combustion conditions. Fuel Processing Technology. 2013;105:20-7.
[104] Dai J, Whitty K. Effects of coal ash on cuo as an oxygen carrier for chemical looping with oxygen uncoupling. Energy & Fuels. 2018;32:11656-65.
[105] Kuo Y-L, Huang W-C, Tseng Y-H, Chang S-H, Ku Y, Lee H-Y. Electric arc furnace dust as an alternative low-cost oxygen carrier for chemical looping combustion. Journal of Hazardous Materials. 2018;342:297-305.
[106] Lyngfelt A, Leckner B. A 1000 mwth boiler for chemical-looping combustion of solid fuels – discussion of design and costs. Applied Energy. 2015;157:475-87.
[107] Pröll T. 10 - fundamentals of chemical looping combustion and introduction to clc reactor design. In: Fennell P, Anthony B, editors. Calcium and chemical looping technology for power generation and carbon dioxide (co2) capture: Woodhead Publishing; 2015. p. 197-219.

Appendix

Table A.1 Species included in the HSCA-database used for global and local thermodynamic calculations in this thesis.

HSC9	**Cr**	**Mn**	**Ni**
As	Cr2(g)	Mn2NiO4(s)	Ni2(g)
As2CoO4(s)	Cr2O(g)	Mn2O4Zn(s)	Ni3O8V2(s)
As2CuO4(s)	Cr2O2(g)	MnO(g)	Cl3Ni(g)
As2Ni3O8(s)	Cr2O3(g)	MnO2(g)	Cl4Ni2(g)
As2NiO4(s)	Cr2O3(g2)	MnO6V2(s)	H3NiO3(s)
As2O3(g)	CrH(g)	Cl3Mn(g)	HNiO(g)
As2O4(s)	CrH2O2(s)	Cl3Mn(s)	**Pb**
As2O4(s2)	CrH3O3(s)	Cl3Mn(s2)	Pb2S2(g)
As2S3(g)	CrO4Pb(s)	Cl4Mn(g)	Pb5Si3O11(s)
As4O10(g)	CrO4V(s)	Cl4Mn2(g)	PbS2(g)
As4O6(s)	CrS2(g)	ClMn(g)	PbS2SiO4(s)
As4O6(s2)	Cl4Cr(s)	ClMnO3(g)	Cl3Pb(g)
As4O6(s3)	ClCr(s)	H2MnO2(s)	H2O2Pb(s)
As4O7(g)	**Co**	HMn(g)	K2Pb(SO4)2(s)
As4O8(g)	'Co10S9'(s)	HMnO(g)	O17Pb12(s)
As4O9(g)	Co2(g)	HMnO2(s)	O19Pb12(s)
As4S6(s)	CO4V(s)	**Mo**	O2Pb(g)
AsH(g)	CO5Pb3(s)	'Mo10O29'(s)	O3Pb2(g)
AsH2(g)	'Co6S8'(s)	Mo2(s)	O3Pb2(s)
AsO2(g)	CoH(g)	MoNiO4(s)	O3PbS2(s)
AsS(s)	CoH2O2(g)	MoO4Zn(s)	O6PbS3(s)
AsS(s2)	CoH3O3(s)	MoS(g)	O6PbV2(s)
C	CoMoO4(s)	MoS2(g)	O7Pb2V2(s)
C2H6O12Zn5(s)	CoO(g)	H2MoO3(g)	O8Pb3V2(s)
C2H6Zn(g)	CoS(g)	HMoO2(g)	**V**
C60(g)	**Cu**	Cl2Mo(g)	Cl3V(g)
C60(s)	Cu2S(g)	Cl2Mo(s)	Cl5V(g)
CCl2S(g)	CuH(g)	Cl2MoO(g)	O10V4(g)
Cl	CuHO(g)	Cl2MoO(g2)	O11V6(s)
Cl4(g)	CuO6V2(s)	'Cl37Mo12'(s)	O13V6(s)
ClHO3S(g)	Cl2Cu(g)	Cl3Mo(g)	O13V7(s)
ClHO4(g)	Cl2Cu2(g)	Cl3Mo(s)	O15V8(s)
ClOS(g)	Cl4Cu2(g)	Cl3MoO(g)	'O5V4'(s)
Cl3(g)	Cl4Cu4(g)	Cl3MoO(g2)	O8V2Zn3(s)
HSC10	Cl5Cu5(g)	Cl4MoO(g)	O9V5(s)
$CuAl_2O_4$	PbS_2SiO_4	Cl4MoO(g2)	H4O7V2(g)
$Cu_2Al_2O_4$	$PbSiO_4$	ClMo(g)	**Zn**
$CuCr_2O_4$	$Pb_5Si_3O_{11}$	ClMoO(g)	H2O2Zn(g)
Ca_2PbO_4		ClMoO2(g)	HOZn(g)
Cu_2PbO_2			HZn(g)
$K_2Pb(SO_4)_2$			OZn(g)
$Pb_3(AsO_4)_2$			ClZn(g)